THESIS FOR THE DEGREE OF DOCTOR OF PHILOSOPHY

High-Performance Full Density Structural and Functional Components

Processing-Microstructure-Property Relationship in PM and AM

ANOK BABU NAGARAM

CHALMERS

Department of Industrial and Materials Science
CHALMERS UNIVERSITY OF TECHNOLOGY
Gothenburg, Sweden, 2024

High-Performance Full Density Structural and Functional Components

Processing-Microstructure-Property Relationship in PM and AM

ANOK BABU NAGARAM

ISBN 978-91-8103-078-5

Doctoral Thesis at Chalmers University of Technology

New serial no: 5536

ISSN 0346-718X

Department of Industrial and Materials Science

Chalmers University of Technology

SE-412 96 Gothenburg

Sweden

Tel: +46 (0)31 772 1000

Printed by Chalmers Reproservice

Gothenburg, Sweden 2024

To my parents

But the pot he was shaping from the clay was marred in his hands; so the potter formed it into another pot, shaping it as seemed best to him.

Jeremiah 18:4

High-Performance Full Density Structural and Functional Components

Processing-Microstructure-Property Relationship in PM and AM

Anok Babu Nagaram
Department of Industrial and Materials Science
Chalmers University of Technology

Abstract

Powder Metallurgy (PM) and Additive Manufacturing (AM) offer resource- and cost-efficient manufacturing for the fabrication of near-net shape components with tailored properties and high precision. These fabrication technologies are regarded as a source of consistent innovation, particularly in the development of new materials and novel processing routes.

This thesis study encompasses both PM and AM technologies, with the objective of investigating their utilization for structural and functional applications. Water-atomized and gas-atomized steel powder grades were used to fabricate the structural components using PM process. Cold isostatic pressing (CIP) process achieves uniform density distribution and enables geometrical complexity through lubricant-free isostatic compaction. The materials included have been the steel powder grade pre-alloyed with 1.8%Cr and admixed with 0.3% graphite and 2% Ni, the Vanadis 4E tool steel, and the FeCrAl powder. To apply CIP, the latter two gas-atomized powders were granulated prior to compaction using an appropriate binder and freeze-drying process.

Sintering of these materials has been achieved to remove the surface oxides. In addition, sintering at high enough temperatures has facilitated the complete elimination of interconnected pores into the components. Hereby, hot isostatic pressing (HIP) has offered a final stage for reaching full density, without the need for capsule. Hence, the combination of CIP, sintering and capsule-free HIP enables the creation of novel components with full density.

The AM technologies enable fabricating complex designs compared to conventional manufacturing methods. Pure copper and 316L austenitic steel are used for the functional applications demonstrated, following the use of powder bed fusion - electron beam (PBF-EB) and powder bed fusion - laser beam (PBF-LB), respectively. Optimized process parameters using melt strategies such as hatch and point melting with PBF-EB resulted in full density with high thermal and electrical conductivity for pure copper. The EBSD analysis revealed the influence of low angle- and high angle grain boundaries on the conductivity of the components. Precision parts of 316L were manufactured as prototype components for waveguide applications using PBF-LB and the geometrical accuracy in the range of tens to micrometers was demonstrated. The feature control capability was depicted by RF resonance frequency measurements and small spread of RF resonance frequency between the samples was shown.

Keywords:

Powder metallurgy, additive manufacturing, Cr-alloyed steel, Vanadis 4E PM tool steel, FeCrAl, pure copper, 316L, high temperature sintering, high density, cold isostatic pressing, capsule-free hot isostatic pressing

PREFACE

This thesis is based on research work performed in the Department of Industrial and Materials Science at Chalmers University of Technology from September 2019 to August 2024 under the supervision of Professor Lars Nyborg and Professor Eduard Hryha. This work has been performed within the framework of project funding from strategic innovation program Metalliska Material through the project DENSE, financed by the Swedish Governmental Agency for Innovation Systems (VINNOVA) and through Centre for Additive Manufacture-Metal (CAM^2) with support from VINNOVA.

This thesis comprises an introductory part on powder metallurgy of steels with a review on aspects related to high density approaches using new processing routes, additive manufacturing and on additive manufacturing of materials for electrification and microtechnology applications and a summary of main research results, which are detailed in the appended papers.

List of appended papers

I. Consolidation Of Water-Atomized Chromium-Nickel-Alloyed Powder Metallurgy Steel Through Novel Processing Routes
Anok Babu Nagaram, Maheswaran Vattur Sundaram, Johannes Gårdstam, Michael Andersson, Zhuoer Chen, Eduard Hryha, Lars Nyborg
Powder Metallurgy, 67(1) (2024) 6-17

II. Effect Of Process Control On The Densification Of Cr-Prealloyed PM Steels Through Vacuum Sintering In Conjunction With Capsule-Free Hot Isostatic Pressing
Anok Babu Nagaram, Eduard Hryha, Zhuoer Chen, Maheswaran Vattur Sundaram, Michael Andersson, Johannes Gårdstam, Lars Nyborg
Conference Proceedings of WorldPM 2022, France

III. Role Of Nickel Addition On Sintering And Microstructure Control Of Chromium-Alloyed Steel Powder
Anok Babu Nagaram, Yu Cao, Maheswaran Vattur Sundaram, Michael Andersson, Hans Magnusson, Eduard Hryha, Lars Nyborg
In Manuscript

IV. Full Density Powder Metallurgical Cold Work Tool Steel Through Nitrogen Sintering And Capsule-Free Hot Isostatic Pressing
Anok Babu Nagaram, Giulio Maistro, Erik Adolfsson, Yu Cao, Eduard Hryha, Lars Nyborg
Submitted for publication

V. Full Density Processing Of Gas-Atomized Spherical FeCrAl Powder By Granulation, Cold Isostatic Pressing And High Temperature Sintering
Anok Babu Nagaram, Eduard Hryha, Lars Nyborg, Erik Adolfsson, Roger Berglund
In Manuscript

VI. **Current Challenges Of Precision Manufacturing Through Powder Bed Fusion - Laser Beam**
Anok Babu Nagaram, Bala Malladi, Lars Nyborg, Lars Manholm, Oskar Talcoth, Ingmar Andersson, Antti Mutanen, and Olli Nyrhilae
Conference Proceedings of Advances in Additive Manufacturing in Powder Metallurgy 2023, USA

VII. **Powder Bed Fusion-Electron Beam (PBF-EB) Of Pure Copper: Effect Of Density And Microstructure On Thermal And Electrical Properties**
Anok Babu Nagaram, Markus Enmark, Phillip Mahoney, Joakim Algardh, Lars Nyborg, Eduard Hryha
In Manuscript

Contribution to the appended papers

Paper I: The author planned the work together with co-authors. Experimental work and analysis of the results was performed in collaboration with the co-authors. The author wrote the paper in cooperation with the co-authors.

Paper II: The author planned the work together with co-authors. Experimental work and analysis of the results was performed in collaboration with the co-authors. The author wrote the paper in cooperation with the co-authors.

Paper III: The author planned the work together with co-authors. Experimental work and analysis of the results was performed in collaboration with the co-authors. The author wrote the paper in cooperation with the co-authors.

Paper IV: The author planned the work together with co-authors. Experimental work and analysis of the results was performed in collaboration with the co-authors. The author wrote the paper in cooperation with the co-authors.

Paper V: The author planned the work together with co-authors. Experimental work and analysis of the results was performed in collaboration with the co-authors. The author wrote the paper in cooperation with the co-authors.

Paper VI: The author planned the work together with co-authors. Experimental work was performed externally by co-authors. Analysis of the results was performed in collaboration with the co-authors. The author wrote the paper in cooperation with the co-authors.

Paper VII: The author planned the work together with co-authors. Experimental work was performed externally by co-authors. Analysis of the results was performed in collaboration with the co-authors. The author wrote the paper in cooperation with the co-authors.

Table of Contents

CHAPTER 1

Introduction

1.1 Background

Powder metallurgy (PM) and additive manufacturing (AM) provide near net or net shape technologies utilized to produce structural and functional metallic components. In 2024 (January), the global PM market was valued at $6.92 billion. At a projected compound annual growth rate (CAGR) of 7.3% from 2024 to 2030, the market size is estimated to reach $10.18 billion [1]. Structural steels find extensive application in the automotive, railway and construction sector owing to their favorable balance of high strength, good fracture toughness and resistance to wear, all achieved at a cost-effective price [2]. For example, synchronizing hubs for automotive gear boxes demand a combination of high mechanical strength and tight dimension control to ensure proper functionality and performance [3].

Additive manufacturing (AM), also known as 3D printing, represents a process for creating three-dimensional objects directly from computer-aided design (CAD) data. This technology utilizes selective consolidation of powder, deposited layer-by-layer in a controlled manner, to fabricate components with intricate geometries that may be impossible to achieve through conventional manufacturing techniques. This advancement in technology has propelled the additive manufacturing (AM) market to a current estimated value of $20.37 billion in 2023, and with expected growth to $88.28 billion by 2030 [4].

The PM technology has grown rapidly due to its unique ability to produce high volumes of complex components with tailored properties, offering an efficient manufacturing approach. One of its main characteristics is to make it possible to fabricate complex product shapes in a cost-effective way. The initial stage of the PM processing sequence involves compaction and shaping. During this stage, micrometer-sized metal particles undergo consolidation to a so-called green body through the application of external pressure, typically uniaxial. This compaction process induces particle rearrangement, mechanical interlocking and plastic deformation at the microscopic level, collectively resulting in the formation of a semi-finished component with sufficient green strength to

handle subsequent processing steps. Effective uniaxial compaction in PM necessitates the use of metal powder with irregular morphology. Water atomization, for example, produces such powder well-suited for this purpose due to its non-spherical shape. The desired geometry is achieved by compaction, whereas to achieve necessary strength the powder compact undergoes a thermal treatment known as sintering. Normally, a delubrication step may be necessary prior to final sintering to remove any lubricants used during powder compaction. The sintering process typically occurs at a temperature range at between 0.7 Tm and 0.95 Tm (where Tm is the absolute melting temperature of the main components in the powder mix in Kelvin degrees) for the specific material. Sintering is conducted within a controlled reducing atmosphere. During this process, atomic scale diffusion at the particle interfaces facilitates the formation and growth of interparticle necks, leading to a significant enhancement in the mechanical strength of the compact.

While PM technology offers excellent dimensional control during fabrication, the mechanical properties of PM components generally are not comparable to those achievable for wrought steels of the same composition due to the presence of residual porosity [5]. A key limitation of PM components stems from their inherent porosity, ultimately leading to a deterioration in the material's overall mechanical strength, thereby compromising its performance for most challenging applications. Many investigations have consistently demonstrated a synergetic effect of density and microstructure on the mechanical behaviour of PM steels [6], [7]. **Figure 1** represents a schematic depicting the relationship between density and various mechanical properties of PM steels. The figure demonstrates that lower density levels typical for conventional press and sinter (range a), pronounces lower mechanical properties, particularly toughness-related properties as impact strength as well as ductility-related as elongation to facture compared to for higher density materials.

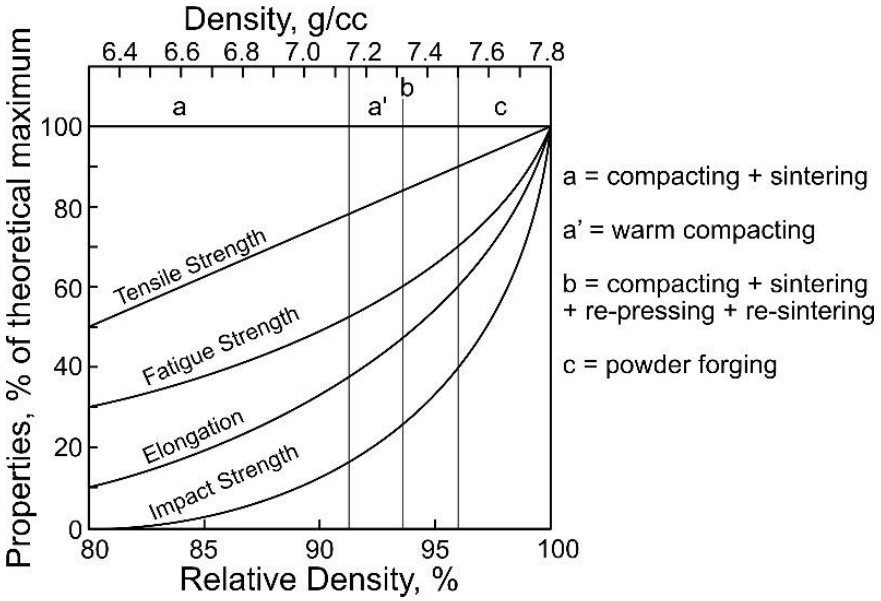

Figure 1. Effect of relative density on the mechanical performance of PM component (redrawn with permission from [7])

In recent years, there has been a surge in demand for high-density PM components within the automotive industry. To address the challenge of porosity and achieve high-density components, a range of advanced powder metallurgy (PM) techniques are being actively explored and implemented. While copper infiltration and powder forging offer established routes to achieving high-density PM components, their application is partly hindered by their effects on the physical nature of the component and additional processing steps associated with these methods, inevitably leading to increased production costs, ultimately impacting the final component price [8].

Achieving high to full density solely by increasing compaction pressure during uniaxial compaction is neither possible nor feasible as the main solution. Conventional uniaxial compaction can achieve near-net density through proper control of alloying elements and uniform distribution of lubricant. Proper lubricant must be chosen with respect to their theoretical densities to avoid its effect on the green density of the compacted parts at high compaction pressure.

Thus, there is interest to avoid/minimize the utilization of lubricant, and novel processing routes must be investigated. In the case of conventional press and sinter route, not only will the die tools and lubricants used affect the cost, but also fabricating complex shapes would be difficult when pressing towards maximum possible compaction density. Alternatively, techniques like double-pressing and double-sintering (DPDS), warm compaction, and high-velocity compaction, coupled with high-temperature sintering, can bring final density towards nominally full densification [9]. Nevertheless, these methods often come at the expense of forfeiting dimensional control and achievable part geometries. Cold isostatic pressing (CIP) is a process where these above-mentioned factors are not necessary and constitute an important part of this study. Cold isostatic pressing (CIP) and hot isostatic pressing (HIP) are also effective methods for densification of large components in medium to low volume production, not necessarily achievable by traditional press and sinter route. However, CIP is limited to achieving near-net shapes with relatively simple geometries, while HIP can accommodate components with intricate features [9]. The HIP is primarily a single-stage process to densify encapsulated powder, but it is also a post-processing technique employed for AM components to eliminate the internal porosity and defects, even though it incurs additional processing costs. Incorporating HIP in any processing route is a viable choice when full density is needed, and any added cost can be tolerated.

To address the challenges of achieving high density while maintaining shaping flexibility, advancements in PM and AM offer promising new approaches, potentially leading to the creation of a new generation of PM and AM components that are both strong and intricately designed. As said, one such processing route within PM field is cold isostatic pressing (CIP) combined with high temperature sintering, followed by capsule-free hot isostatic pressing (HIP). Recent process advancements in HIP technology have enabled the integration of the heat treatment step within HIP cycle, resulting in a more potentially cost-effective process [10]. The AM also offers promising routes with methods like powder bed fusion – electron beam (PBF-EB), powder bed fusion – laser beam (PBF-LB),

binder jetting (BJ), directed energy deposition (DED), and lithography-based metal manufacturing (LMM). These techniques unlock design freedom by enabling the fabrication of functional components with intricate geometries, thereby overcoming the limitations of traditional PM compaction in terms of geometric complexity [11]. Structural applications are often a key concern in the development of these AM processes, but surely, they are also of increasing interest to accomplish functional applications as further outlined below.

In summary, the behavior of metallic materials is primarily determined by porosity and microstructure, which encompasses the volume fraction and distribution of the constituent phases, grain size, and grain boundary orientation [12], [13], [14]. Achieving an optimal balance among density, microstructure and geometry ensures materials performance in both structural and functional applications. This approach requires the exploration of advanced manufacturing processes for these applications.

1.2 Research Objectives and Approach

This thesis study addresses the possible advanced manufacturing processing routes of metallic materials for structural and functional applications. Specifically, it focuses on:

- Elucidating the influence of novel processing routes and sintering on the microstructure and potential properties of powder metallurgy (PM) steels.
- Evaluating the effect of process parameters on the quality and performance of additively manufactured (AM) components with focus on functional performance.

1.2.1 Powder Metallurgy (PM)

Figure 2 below shows the processing route of PM technology utilized in this study which allows improved densification through freeze granulation (FG), cold isostatic pressing (CIP), followed by solid state sintering or liquid phase sintering (LPS) and capsule-free HIP. The processing enables the materials to reach relative density levels of 95-99.5% after sintering depending on material system, followed by capsule-free hot isostatic pressing to reach nominally full density. For this processing route, the research questions are depicted as follows.

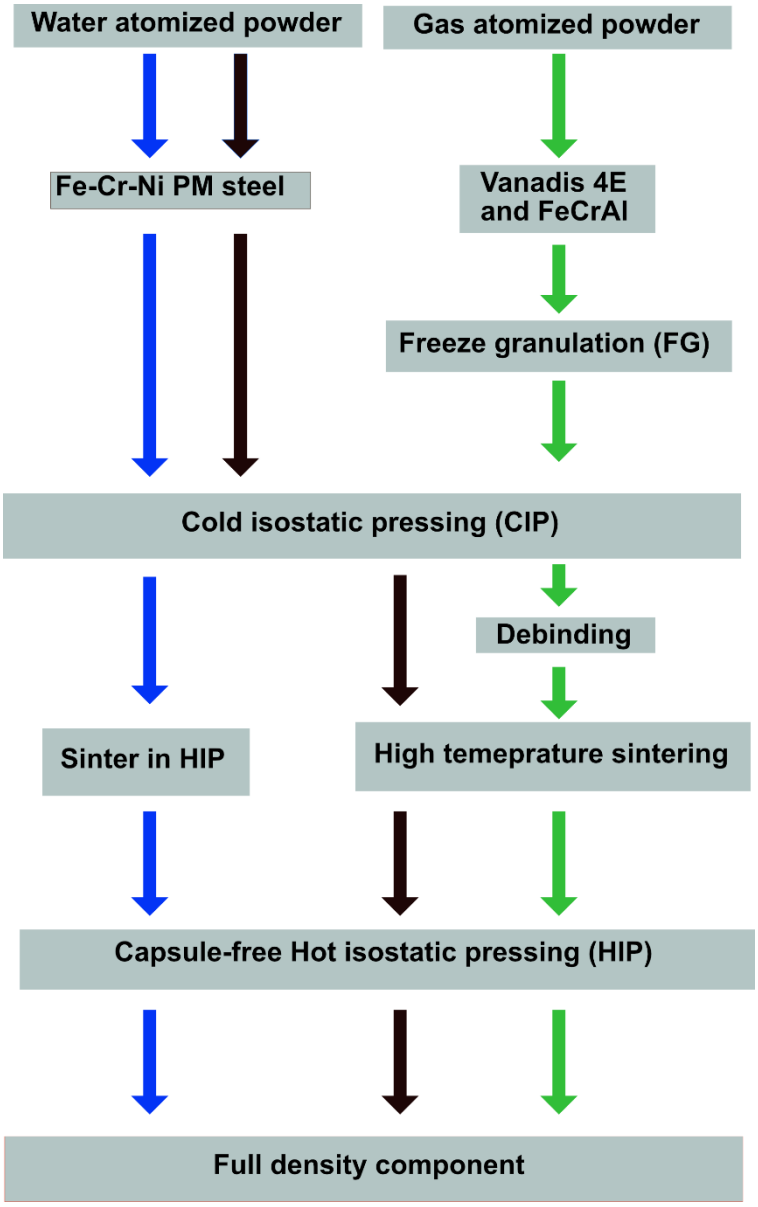

Figure 2. Research approach for PM steels.

RQ1: *How can the processing route be tailored to achieve full densification Fe-Cr-Ni PM steel water atomized steel powder?*

RQ2: *How will alloying by admixing Ni affect sintering of Cr-alloyed water atomized steel powder?*

RQ3: *How can processing route and sintering be tailored to achieve full density components starting from gas-atomized Vanadis 4E tool steel powder or FeCrAl powder?*

1.2.2 Additive Manufacturing (AM)

Additive manufacturing AM) offers exceptional design freedom, enabling the creation of complex geometries that can achieve good mechanical performance. This unique combination makes AM a compelling choice for fabricating functional components from many metallic materials. Here focus is placed on pure copper and 316L stainless steel to explore functional properties and feature control rather than mechanical properties as such, involving research questions as follows.

RQ4: *What are the challenges in producing precision components for functional applications using PBF-LB with particular reference to waveguides?*

RQ5: *What is the effect of melt strategies (hatch vs. point) in powder bed fusion – electron beam (PBF-EB) on the densification, thermal and electrical conductivities?*

CHAPTER 2

Powder Metallurgy and Additive Manufacturing

2.1 Past to Current Trends in Powder Metallurgy and Additive Manufacturing

The origins of powder metallurgy (PM) stretch back to 3000 B.C, with its applications evident in artifacts from this era, such as the Iron pillar of Delhi and monuments from the Egyptian civilization. This long-standing practice demonstrates the enduring value of PM techniques [5]. Although, the methods for powder production during this era remain unclear, the available evidence suggests that the resulting reduced sponge metal powder was likely consolidated through hammered or forged techniques to produce PM tools. Due to the absence of knowledge in furnaces then, likely restricted high temperature melting of metals processes. Consequently, metals with comparatively lower melting points, such as gold and bronze, were preferentially employed for decorative applications. Progressive advancements in furnace technology facilitated the melting of metals with high melting points. The mid-20th century experienced a significant surge in the powder metallurgy (PM) industry, particularly in the production of automotive components like self-lubricant bearings [15]. In recent days, PM industry has been widely used in various applications such as automotive [16], fuel cells [15], [17], soft magnetic composites [18], and high-performance components [19]. The PM technology plays a dominant role within the automotive industry, accounting for an estimated 60-70% of all PM-produced components globally [16].

The PM technology offers a unique advantage of tailoring the microstructure of PM steels. This control is achieved through meticulous selection of powder characteristics such as size, shape and composition and controlled optimization of sintering parameters such as temperature, time and atmosphere. This approach facilitates the development of desired microstructures, which are critical for achieving enhanced strength, improved toughness and good fatigue resistance [20], [21], [22]. As the research continues to explore advanced PM techniques for high-performance applications, AM technology enables

now a new route for the creation of complex geometries and functional graded components.

Additive manufacturing (AM) technology which is also known as rapid prototyping or 3D printing is a process in which material is deposited to fabricate a 3-dimensional object from a computer-aided design (CAD). The concept of AM emerged from the demonstration of photosculpture technique developed by Francois Willeme in 19th century which involved 24 cameras arranged in a circular manner to capture an object's profile from 360° angles [23]. Later, in 20th century, first rapid prototyping technology was demonstrated and developed by Kodama, Japan, in which 3D plastic components are fabricated using photo-hardening polymers with UV exposure [24]. The challenges of complexity and customization demanded by various applications have driven significant advancements in AM technology. Following which the development of AM technology expanded to stereolithography apparatus (SLA), fused deposition modeling (FDM), sheet lamination, material extrusion, material jetting (MJ), Vat photopolymerization, directed energy deposition (DED), binder jetting (BJ), powder bed fusion – laser beam (PBF – LB), powder bed fusion – electron beam (PBF – EB) and [25], [26], [27], [28], [29], [30], [31], [32], [33], with metal powder-based an important of the latter four technologies in particular.

2.2 Fabrication of Metal Powder

2.2.1 Water Atomization (WA)

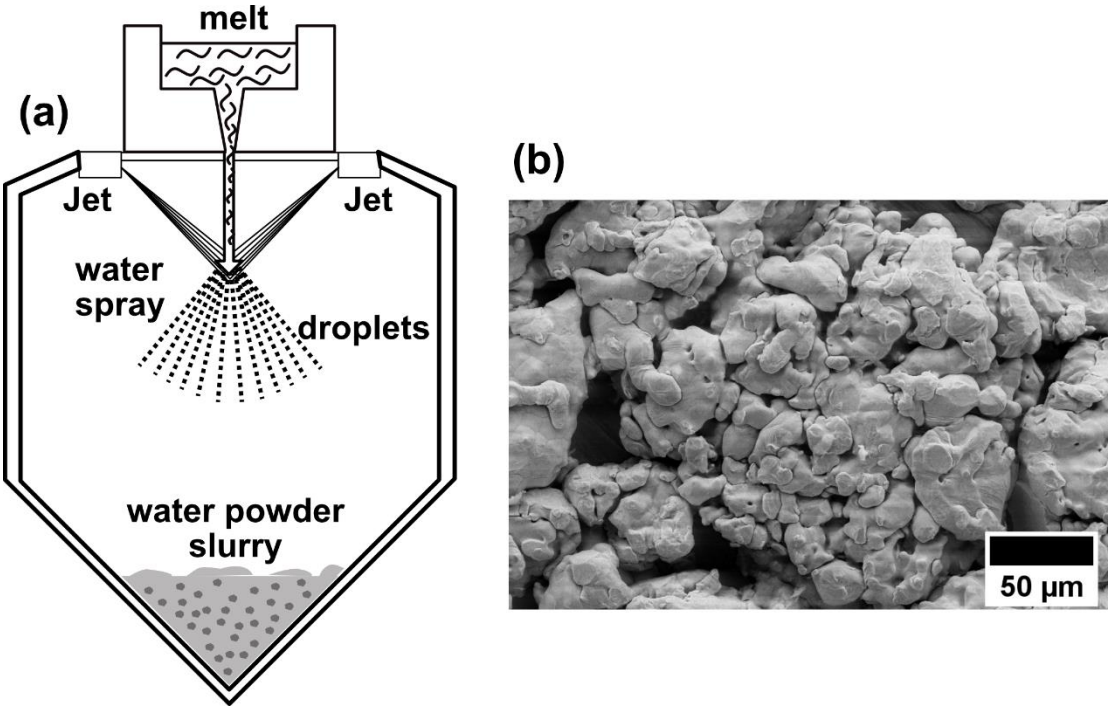

Figure 3. (a) Schematic of water atomization process , and (b) SEM image of water atomized low-alloy steel powder.

Water-atomization is a cost-effective methodology primarily used to produce iron, low-alloy iron and steel powder for pressing and sintering in the PM industry. The molten metal is poured into the tundish either directly or by means of a ladle. This process is effective by striking the molten metal running through the nozzle of a tundish with high pressure water jets. This forces the molten metal to disintegrate into droplets and rapidly freeze forming powder in irregular shapes. A schematic of the water atomization (WA) process and irregular shaped steel powder produced through WA process is shown in **Figure 3**.

The water-powder slurry is collected in the dryer to remove the water content prior to annealing to soften the metal particles and reduce the surface oxides formed during atomization. The content of oxygen in water-atomized powder is primarily an effect of its irregular shape and associated high specific surface area [34], [35]. In fact, previous studies revealed that typical water-atomized pre-alloyed steel particles are covered mainly by 3-7 nm of homogeneous thin iron-rich oxide layer, together with small amount of thermodynamically stable oxide particulates with average size of 200 nm spread on the surface [36], [37], [38]. The irregular shape of water atomized powder enhances compressibility due to better interlocking between particles, resulting in high green strength.

2.2.2 Gas Atomization (GA)

Gas atomization is the process in which a stream of molten metal is dispersed by a high-velocity jet of air, nitrogen, argon or helium. This pressurized gas jet flowing out of a nozzle is used to break up a molten metal stream into fine droplets as shown schematically in **Figure 4** below. The suitable gas is selected based on cost, thermal conductivity and how it interacts with the alloy [39]. Inert gases are used for reactive metals such as titanium and nickel-based alloys.

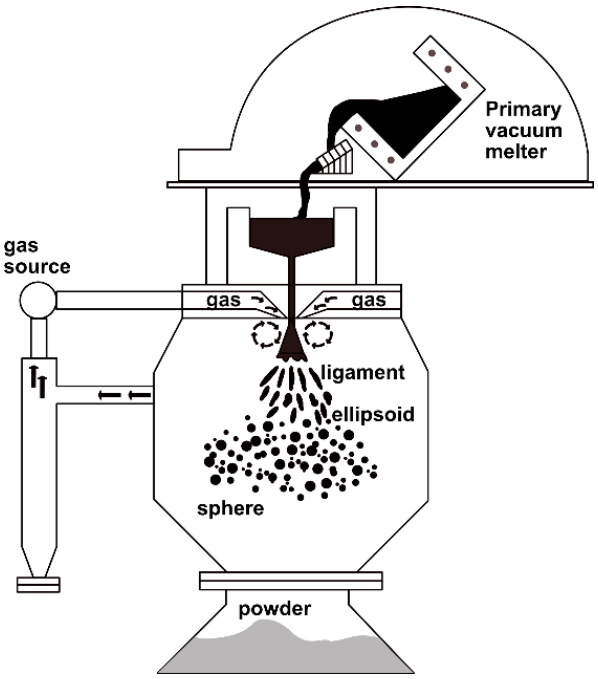

Figure 4. Schematic of Gas atomization process.

The particle size is controlled by gas-to-metal ratio in GA process while the water jet pressure together with various process parameters determines the size in WA process [40]. The powder obtained by GA process has close-to-spherical shape with relative smooth surfaces. The GA is a high-production process while achieving low oxygen content and increased packing density of the material. The GA powder lacks the necessary interparticle forces for effective compaction, thus surface-active additives and organic binders are used to enhance the green strength which is essential for compacts of intricate shapes [41].

2.3 Alloying Methods

During recent years a lot of effort has been put into developing low alloy PM steel components. Alloying of the materials is done to boost the mechanical properties of the final product. High strength is the main prerequisite property for these steels to be produced to compete with the traditional alloys. Depending upon the nature of alloying elements in the alloy, various procedures have been established to produce low alloy systems as shown in **Figure 5**.

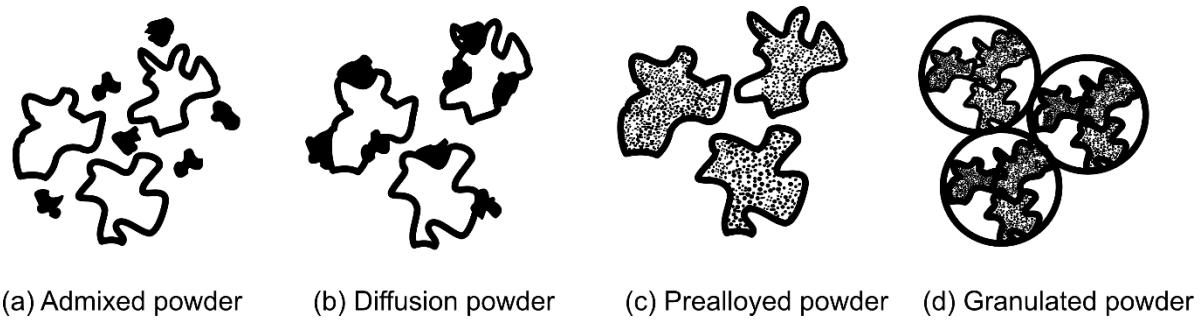

Figure 5. Schematic illustration of alloying elements using different alloying methods.

2.3.1 Admixed Powder Grades

Alloys are produced by mixing elemental powder to the base powder, which does not compromise the compressibility in uniaxial pressing [42]. This is a result of the fact that the mixture is not a product of prealloyed system, which otherwise increases the resistance to plastic deformation owing to e.g., solution hardening of the metal matrix thus reducing the compressibility. Constituents with weak affinity towards oxygen can with ease be admixed such as graphite, nickel, copper, etc. Nevertheless, the degree of alloy homogenisation during sintering is limited due to too slow diffusion of substitutional alloying elements like e.g. nickel at sintering temperature.

2.3.2 Diffusion-alloyed Powder

Fine elemental powder of e.g., nickel, copper and in some cases also molybdenum is admixed to the iron/steel base powder and bonded to the surface of the base powder by solid state diffusion process termed diffusion alloying. The bonding is controlled during the diffusion alloying heat treatment with resulting powder mixture known as “partially

prealloyed mixture" [42], [43]. This approach is performed to retain compressibility by restricting the alloying in the pre-alloyed state of base powder.

2.3.3 Pre-alloyed Powder

Additions of elements to the molten metal in the atomization process results in a chemically uniform distribution of alloying elements in the alloy [40], [42]. Low alloy steel powder with not more than two major alloying elements is often the case and the composition is specifically formulated for high performance PM parts. Elements that have high affinity towards oxygen such as Cr are commonly pre-alloyed with iron base system. The pre-alloying lowers the activity of the elements compared to having elements like Cr and Mn in elemental powder form, hence means less challenge in sintering control.

2.3.4 Hybrid-alloyed Powder

Addition of elemental powder or master alloy powder to either diffusion-alloyed or pre-alloyed powder are called hybrid-alloyed powder systems [44]. These new hybrid-alloy powder grades are formulated to obtain required chemical composition and attain improved microstructure and properties on sintering at high temperatures.

2.4 Granulated Powder (Freeze Granulation)

Alloy powder that is not possible to compact to necessary green strength due to either alloy system characteristics or their spherical shape, i.e., powder produced by means of gas atomization, can be granulated by mixing with binder resulting in enough green strength after pressing. These granules are free-flowing and do not agglomerate, and one way of producing them is by using the technique called freeze granulation [45]. A suspension with powder is then sprayed into liquid nitrogen (-196 °C) bath to be freeze-dried. This produces powder-containing droplets without voids. These droplets are then dried in vacuum through sublimation, which helps in the formation of spherical powder granules. Parameters responsible for the granule size distribution are air pressure, rheology of the suspension and the pump speed used during the spraying stage. A schematic of freeze granulation technique is shown below in **Figure 6**.

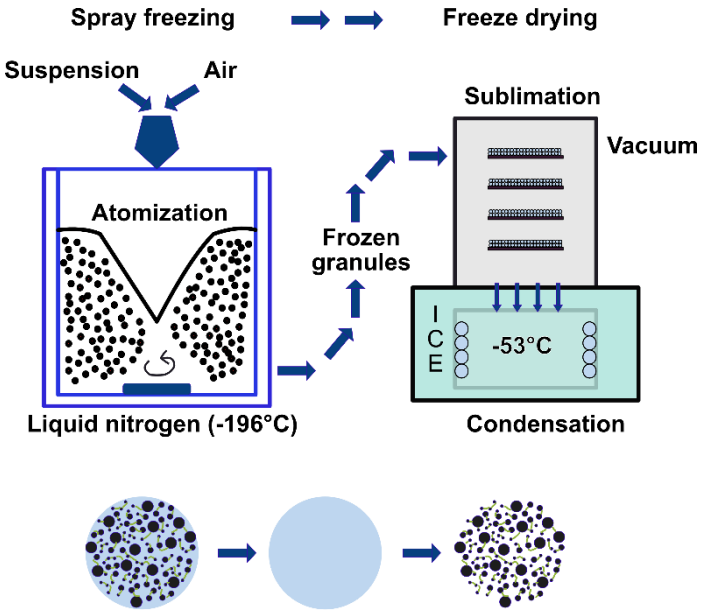

Figure 6. Schematic of freeze granulation technique.

2.5 Processing

An important aim of PM is to achieve as high relative density of the component as possible. High relative density is a requirement because with increase in density, mechanical properties such as strength, ductility and toughness are significantly improved [46].

2.5.1 Uniaxial Compaction

Uniaxial compaction is a widely used method in PM industry for producing structural components. In addition to the above-mentioned parameters in section 2.5, the lubricant admixed with water-atomized powder when filled in the die and compacting uniaxially influences the densification of the powdered material. The use of low-density lubricants will take up much of the compact volume, affecting the reachable sintered density after the removal of lubricant [47]. In conventional pressing process, there is also density gradient caused by a non-uniform pressure distribution within the compact along the die walls, with decreasing gradient along lateral direction from the surface to the core of the part. This is a result of mainly the friction between the powder and die wall in combination with the effect of interlocking particles, thus having impact on dimensional tolerances after sintering. Although addition of lubricant improves compressibility, reaching high relative density after sintering after uniaxial compaction is not easy [47], [48], [49]. It is possible to approach uniform distribution of density within the compact by moving the punches relative to another with regards to the desired density of the component having different sections using platens [50].

2.5.2 Cold Isostatic Pressing (CIP)

Cold Isostatic Pressing (CIP) is a process in which isostatic pressure is applied as shown in **Figure 7** below, on the powder body resulting in uniform density distribution within the compact fabricated, normally resulting in low distortions during sintering. The CIP process is carried out using a pressure medium such as liquid or air at between 100 MPa to 600 MPa at room temperature for some minutes, typically e.g., 2 minutes. The CIP process can be performed in two ways (a) wet bag isostatic pressing (b) dry bag isostatic pressing. In the wet bag isostatic pressing process, flexible rubber mould design shaped to final product is filled with powder and the mould is then vacuum sealed in a bag. This bag is placed in the CIP chamber containing pressure medium. In dry bag isostatic pressing process, powder is directly filled into the tool which is fixed to the CIP chamber containing pressure medium. CIP provides an advantage compared to conventional pressing as there is no friction between the metal particles and die walls. Hence, there is no need for lubricants, provides for economical tooling cost (wet bag), possibility for large parts in size (wet bag), compacts with complex shape and in fact comparably high production rate (dry bag). In addition to other PM technologies, CIP process is characterized by low energy consumption, thus low production costs of at least 60% when compared to conventional manufacturing routes [51], [52], [53], [54].

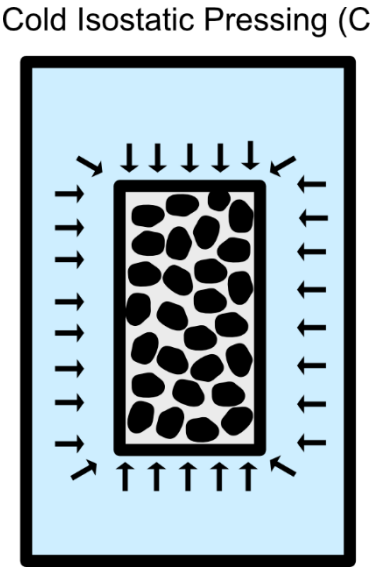

Figure 7. Schematic of cold isostatic pressing (CIP).

2.5.3 Delubrication/Debinding

One of the main concerns during uniaxial compaction is the friction between the powder and die wall, which significantly influences the density gradients within the pressed part, in combination with tool wear. As discussed in earlier section 2.5.1, additives such as lubricants are either admixed to the powder or applied on the die wall to increase the compressibility during the compaction and minimize the tool wear. Depending on the type of additives admixed to the powder in case of Cr-alloyed grades, lubricants are

evaporated or decomposed to heavy hydrocarbons at around 450 °C in dry nitrogen atmosphere during delubrication stage [55], [56], [57], [58], [59]. In **Figure 8** a schematic representation of delubrication process is shown as the lubricant escapes from the surface of the green part [60]. Gas-atomized powder is difficult to compact through uniaxial compaction, thus a binder is used to hold the powder together [57], [61]. The binder provides excellent shape retention during compaction and enhances the strength of the pressed components [45]. It is defined that temperature above 500 °C, should allow complete removal the binder through degradation during debinding process for steels [62], [63] .

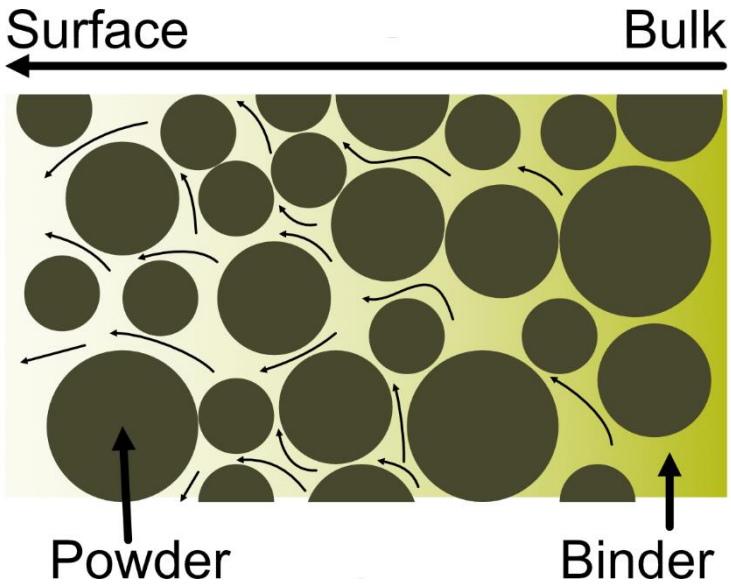

Figure 8. Schematic representation of the debinding process of a green part.

2.5.4 Sintering

Solid State Sintering

Sintering is defined as a process of heat treatment aiming at bonding metal particles of a pre-shaped compact at an elevated temperature that is below the melting temperature, in the range of 70% to 90% of the melting temperature of the main element in Kelvin degrees. The fundamental driving force of the sintering process is to decrease the surface free energy which is caused by surface transport and bulk transport mechanisms as can be seen in **Figure 9**. In the first stage, growth of sinter necks is dominated by surface diffusion and evaporation-condensation mechanisms, which contribute to transfer of matter to the sinter necks without leading to shrinkage and densification. Bulk transport during sintering plays a key role in promoting the growth of necks between particles, leading to material shrinkage and densification.

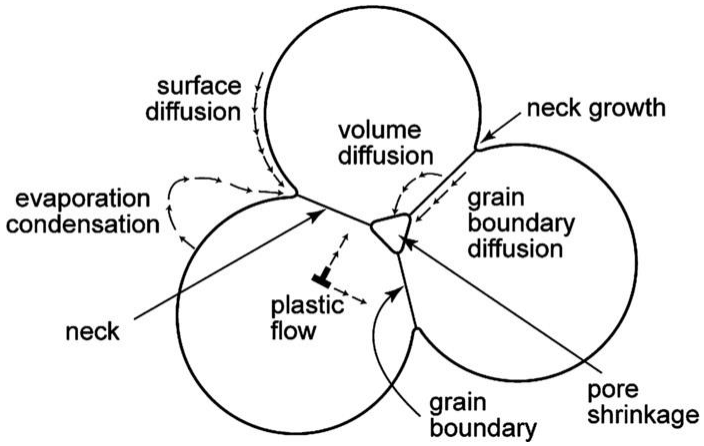

Figure 9. A schematic representation of spherical powders showing various sintering mechanisms Ref. [64].

Sinter necks are formed in the first stage at the contact of metal particles during sintering and later, grow as the sintering temperature/time increases with resulting densification due to the predominant bulk transport mechanisms such as volume diffusion and grain boundary diffusion. Surface diffusion and grain boundary diffusion are more rapid diffusion mechanisms that are active at comparably lower temperatures compared to volume diffusion and hence particularly involved in initial sintering stages. Intermediate stage involves pore isolation contributing to densification. In the later stage of sintering, with increase in temperature, pores are not only reduced in number, but also change their morphology to become more rounded [65]. With the increase in sintering temperature, porosity is decreased, i.e. sintered density is improved, thus resulting in enhanced mechanical properties [66].

Grain growth takes place as the pores evolve with increase in sintering temperature. This coarsening of grain size will influence the properties of the material. Thus, controlled microstructure having finer grain size with high density results in the improvement of the sintered properties. Shrinkage of pre-shaped compacts is one of the key factors of sintering, which influences the shape and dimensions of the sintered compact. Higher green density after compaction will lead to lower shrinkage to reach the given sintered density and this improves the ability to reach desired final dimensions.

To achieve proper neck growth between the metal particles during sintering, these must be fully or partially free from surface oxide, otherwise sinter neck formation will be hampered [67]. The role of surface oxide characteristics on sintering of steel powder has been extensively studied [36], [68], [69]. In conclusion, it is shown that such powder is mainly covered by 3-7 nm, Fe-based oxide layer and to minor amount by particulates formed by more stable oxides rich in strong oxide formers as Mn and Cr [36], [69], [70]. Oxide reduction during controlled sintering helps in achieving effective necking and avoids the growth of thermodynamically stable oxides [71]. Since the atmosphere in the furnace greatly affects the compacts during sintering, it must be performed either at inert, reducing or vacuum conditions. The predominance of Fe-oxide with respect to

surface coverage means that most of the surface oxide can be reduced in an early stage already during the heating state of the sintering, while the Cr- and Mn-rich oxides can only be affected at higher temperatures during the sintering [56], [58], [70], [71].

Liquid Phase Sintering (LPS)

In LPS, a liquid phase coexists with solid grains during sintering. During heating, powder mixture undergoes solid state sintering, which significantly increases the densification. Once the liquid is formed, LPS can be divided into three stages: particle rearrangement by liquid flow, solution-reprecipitation and solid-state sintering, as shown in **Figure 10** [72]. The liquid formed creates a capillary force promoting mobility and rearrangement between solid particles, which accelerates the formation of strong interparticle bonds. As the contribution of rearrangement to densification diminishes, it paves the way for solution-reprecipitation stage to become dominant in solubility and diffusivity. The wetting phenomenon in LPS is due to the solubility of solid grains in the liquid. The lower solid-liquid surface energy compared to solid-vapour surface energy, creates a thermodynamic driving force for the system to favour contact between the solid and liquids phase, resulting in a lower overall system energy. In addition, smaller grains exhibit higher energy and solubility compared to the larger ones. Thus, this solubility differences as a function of grain size creates a concentration gradient of the solute species in the liquid. Upon reaching the solubility limit in the liquid, diffusion from small grains to large grains contributes to precipitation of solute species (reprecipitation) on the larger grains. This phenomenon, results in grain coarsening, along with densification through grain shape accommodation [72], [73]. During intermediate stage, grain coarsening and shape accommodation are driven by a desire to minimize the system energy. This reduces the interfacial area between the grains, thus resulting in concurrent microstructural changes. Although pore filling is associated in the final step of intermediate stage, their elimination required grain growth and grain shape accommodation. In the final stage, grain growth continues together with grain shape accommodation as pores are eliminated. The final microstructure obtained during the final stage impacts its properties like wear resistance, strength, fracture toughness, electrical characteristics [74]. The LPS is classified into two categories: (a) transient liquid phase sintering and (b) persistent liquid phase sintering. In transient LPS, the powder consisting of solid base mixed with additive which has a lower melting point, forms a liquid phase at the beginning of the sintering. As sintering progresses, this liquid content gradually disappears to completely zero [75], [76]. In persistent LPS, liquid content remains at the sintering temperature and solidifies during cooling producing desired microstructure with tailored properties [72]. Super-solidus liquid phase sintering (SLPS) is a variant of persistent LPS, where the liquid phase is formed in a pre-alloyed powder instead of via mixed powder as in traditional LPS, when heated to temperature between solidus and liquidus [74].

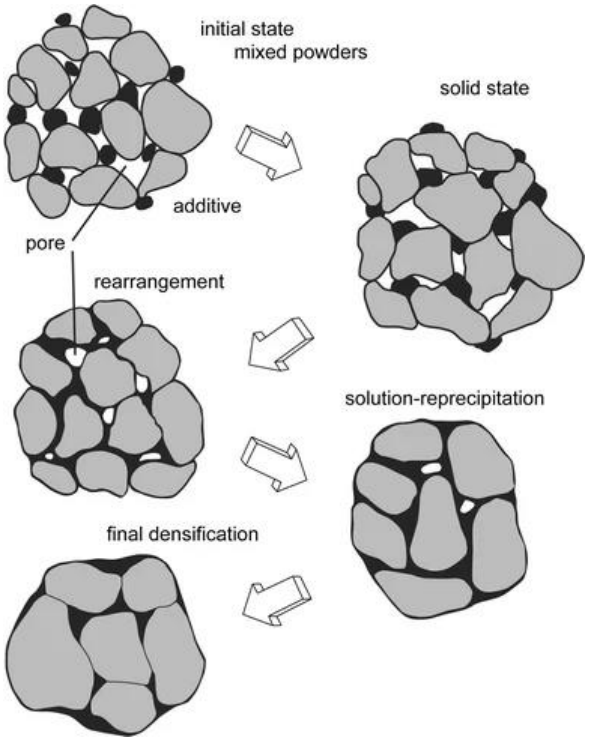

Figure 10. A schematic of the powder mix during liquid phase sintering, Ref. [72].

High Temperature Sintering (HTS)

Density is one of the main characteristics that influences material properties. High performance parts require enhanced strength which is achieved with high sintered density [5]. Previous studies have shown that increase in sintering temperature for Cr-alloyed PM steels results in higher density [65], [77], [78], [79], when sintering at 1250 °C densification increases by up to 1% of the theoretical density in relation to that achieved at 1120 °C. At the higher temperature, the pores tend to become isolated and show more roundness. The temperature of 1120 °C is otherwise most widely used in industry for sintering PM steels using conveyor belt furnace. Such furnace types are restricted to work at around this lower temperature. Thus, batch furnaces are developed for high sintering temperatures including e.g., low pressure sintering furnaces (low vacuum sintering). It should be noted that with an increase in temperature, increased dimensional changes are observed for the same material when sintered either in reducing atmosphere or in vacuum. In addition, increase in temperature also tentatively influences the density of the material as the reduction of stable oxides is eased at higher temperatures for given sintering atmosphere, resulting in stronger neck growth and tentatively improved mechanical properties [69], [80].

Gaseous Sintering

The fundamental purpose of controlled atmosphere during sintering is to prevent oxidation and to reduce surface oxides, which results in good bonding between the adjacent metal particles. In Ferrous PM industry, three main sintering atmospheres are traditionally used: reducing-decarbonizing (e.g., dissociated ammonia, hydrogen), reducing-carbonizing (e.g., endogas) and inert (e.g., nitrogen). In modern sintering,

nitrogen-hydrogen mixtures and vacuum sintering are between the most used. For the reduction of wüstite (FeO) at normal sintering temperature of 1120 °C, the dissociation pressure of about 10-12 atm. is required to decompose FeO without active reducing agent, unless done at ultra-high vacuum conditions [81]. Still, as soon as there is hydrogen in the sintering atmosphere the Fe2O3 layer on the powder surface is readily reducible at below 400 °C. In case of Cr-alloyed PM steels, the sintering in hydrogen-containing atmospheres means that action of hydrogen is often not strong enough to impact on the Cr-Mn-oxide particulates, which means that carbothermic reduction driven by the carbon added to provide the carbon level of the material instead becomes decisive [36], [58], [70].

Vacuum Sintering

Processing in vacuum during sintering is termed as vacuum sintering. Recent studies showed that Cr-alloyed PM steels can be well sintered in low vacuum and significant impact on the reduction of oxides have been obtained due to carbothermal reactions occurring at temperatures of above 1000 °C [71]. Materials like titanium, tool steels, stainless steels and magnetic alloys are sintered in vacuum as these materials react during sintering in atmospheres containing e.g., nitrogen. In case of vacuum sintering, it is important to maintain back pressures above the vapour pressures of the constituents of the alloy. If not so, sublimation is expected, which influences the material stoichiometry and leads to furnace contamination with changes observed in sintering behaviour [82].

2.5.5 Hot Isostatic Pressing (HIP)

Hot isostatic pressing (HIP) is a process involving the application of high temperature and high isostatic pressure. The pressure is accomplished using inert gas as a transfer medium, also previously referred as “gas pressure bonding”. In this process, powder is filled in metallic canister, which is placed in the HIP chamber to obtain full densification by the combined action of temperature and pressure [83], [84]. One of main advantage of the HIP process is achieving fully densified components at lower temperatures (e.g., 1100 °C-1150 °C) due to high isostatic pressure when compared to conventional sintering process, for which high temperature sintering (1250 °C or higher) is required to at least reach closed porosity. The HIP procedure helps in preventing or limiting the addition of sintering aids and grain-growth inhibitors. Uniformly dense components are produced with large length-to cross section ratios, weighing from less than 100 g to 30 tons reaching full relative density of the material with respect to its theoretical density. In addition, material used for canister should be like the alloy matrix and there is quite some effort to create the canister, making it an expensive process.

Capsule-free Hot Isostatic Pressing

The HIP can be used on the pre-shaped component without using canister as shown in **Figure 11**. This, however, requires materials prior to HIP that are free from surface pores that do not provide pore channels into the part, otherwise achieving full density is not

possible. Furthermore, to reach high quality material using capsule-free HIP, it is important to eliminate the effect of oxide content resulting from the surface oxide of the atomized powder. This is in particular important for water-atomized grades that have high surface oxygen content owing to their high specific surface area. Typically, Cr-alloyed steel powder has an oxygen level of 0.15 wt.% [85]. If this oxygen level is not substantially reduced, it can lead to a degradation in mechanical properties. This happens when oxide inclusions are present at the contact between the particles, deteriorating the properties such as ductility, fatigue resistance and impact toughness [86], [87], [88], [89]. Consequently, a controlled processing route is required, and this can be achieved with precise control along the whole processing route, eliminating interconnected pores and oxides during the sintering process [90]. This methodology is already applied to parts produced by MIM and sinter-based AM [91]. Although the HIP is done in argon gas for a capsule containing material, it is not necessarily recommended for capsule-free HIP proceeding of a conventionally sintered component. This is because argon might get trapped in the material with risk for residual argon-induced porosity. Hence, new approaches of sintering in vacuum and continuous capsule-free HIP are developed in this thesis study.

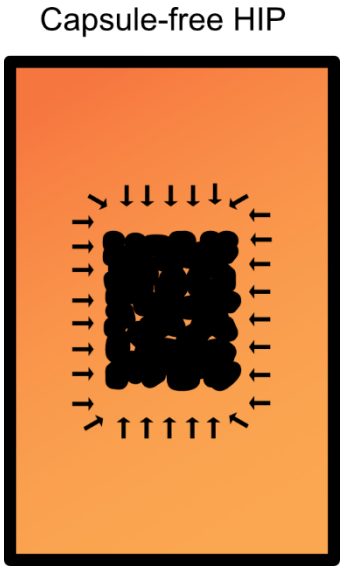

Figure 11. A schematic illustration of capsule-free hot isostatic pressing (Capsule-free HIP).

2.5.6 Powder Based Metal Additive Manufacturing

Metal Additive Manufacturing (AM) offers an advanced and effective approach for the innovative fabrication of metallic components. AM also known as 3D-printing, is a process that involves successively depositing metal powder layer by layer to create a three-dimensional component from a three-dimensional Computer Aided Design (CAD) [92]. AM covers a number of technologies that are classified into many ways depending on the material feedstock, energy source used such as laser beam, electron beam, or material deposition technology, etc.

Powder Bed Fusion

Powder bed fusion – laser beam (PBF – LB) and powder bed fusion – electron beam (PBF-EB), use laser and electron beam as thermal source to fuse the metal particles together at a specific region on each layer added to the previous one. **Figure 12** shows the schematic representation of the working principles of PBF-LB and PBF-EB processes. Controlled process parameters in both technologies significantly impacts the quality of the final components. These parameters can be categorized into three segments such as powder parameters, machine parameters, laser parameters for PBF-LB, as well as electron beam parameters for PBF-EB. Gas-atomized powder exhibits good powder packing density influenced by powder size distribution, and powder flowability determined by powder flow characteristics due to their spherical morphology [93], [94].

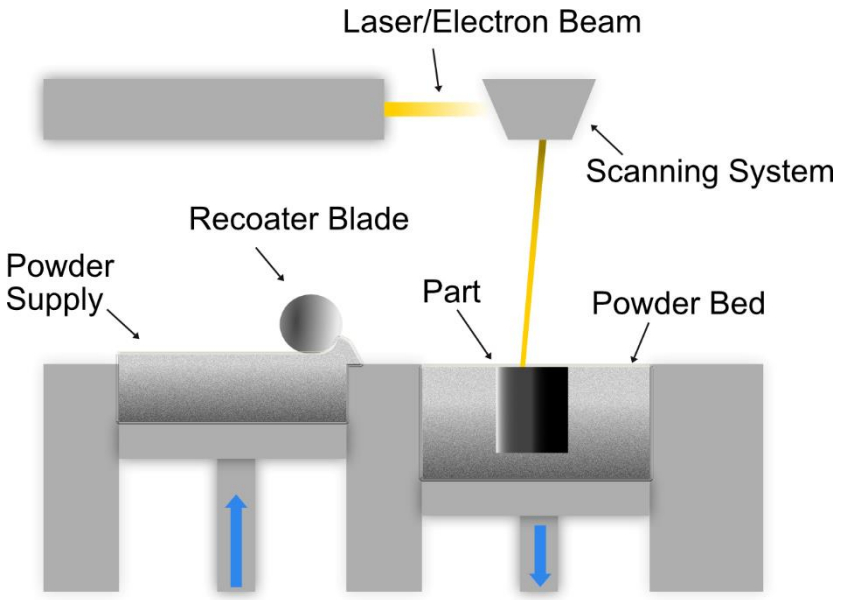

Figure 12. Schematic illustration of the powder bed fusion - laser beam and electron beam processes.

CHAPTER 3

Control of Density, Microstructure and Geometry for Performance

In recent years, PM and AM industry has drawn attention towards materials of interest for high performance applications. This indicated that components for various applications such as structural and functional, need to fulfill certain requirements. A proper balance between property, microstructure and geometrical tolerance is required for materials manufactured for specific applications such as structural and functional, as illustrated in **Figure 13**.

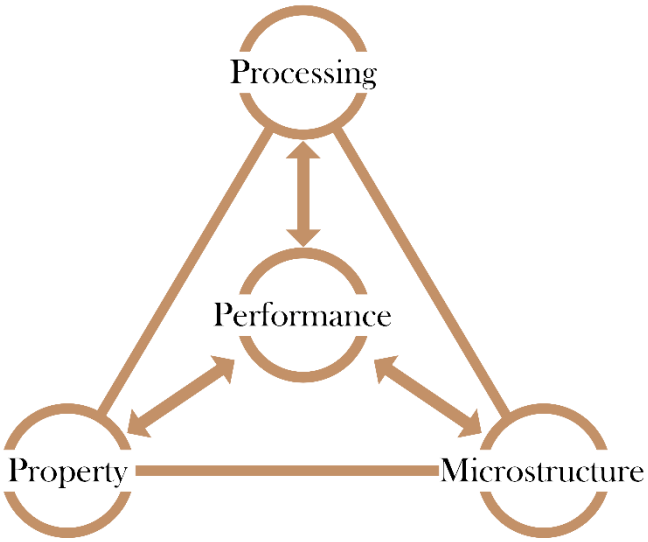

Figure 13. An overview of the PM and AM components demonstrating a balance between property, microstructure and geometry to obtain better performance.

3.1 Density for High-Performance Structural Components (WA and GA powder)

In PM, density plays a significant role for achieving high performance components. In this study, the main challenge is to produce high density components through novel approaches together with tailoring the microstructure for high performance. This study explored the sintering aspects of Cr-alloyed PM steel, cold work PM tool steel and high temperature resistance FeCrAl PM steels to enhance the density of potential components and hence increasing strength of high-performance materials.

As described earlier, bonding between the metal particles during compaction is necessary to facilitate shaping and achieve superior mechanical strength after sintering. A compacted part requires a minimum level of green strength to withstand further handling without damage. Particle morphology: shape and size distribution significantly affect the powder packing behaviour, including flowability and compressibility. Compressibility is further influenced by intrinsic material properties like composition, hardness, particle size, and as well as extrinsic factors like the presence of lubricants [95]. Several approaches to achieve increased densification have been studied through high velocity compaction, double press-double sinter, uniaxial compaction followed by sintering and HIP, and liquid phase sintering [9]. Irregular shape particles produced through water atomization technique, exhibit good green strength compared to spherical ones [8], [95], [96], [97]. The application of the increasing compaction pressure leads to a concomitant rise in green density. Hence, enhanced particle coordination achieved through compaction promotes densification during sintering [98]. Lubricants are used to minimize the interparticle friction between the metal particles by admixing and to reduce the frictional forces between the compaction tool surface and metal particles by being redistributed to tool wall or when possible, by being applied directly to the die wall [8], [47], [99]. Clearly, one of the main challenges of uniaxial compaction is the complexity in achieving uniform distribution of densification within the compact, owing to the friction between the powder and die wall. On the other hand, cold isostatic pressing allows reasonable geometrical flexibility, no use of lubricants and compaction die tools. Isostatic pressed compacts promote more even densification in the entire cross section of the sample, thus resulting enhanced green strength exhibiting 50% more than uniaxial compaction carried out at the same pressure [52], [53], [54], [100]. Consolidation of hard powder particles with spherical shapes such as PM high alloyed steels is difficult for uniaxial compaction because of its high hardness [101]. Hence, the most suitable compaction procedure to achieve high densification for PM structural components is by admixing binder to such powder, thus increasing the compressibility during isostatic pressing [61].

Dominance of open and interconnected pores is more effective on the mechanical properties than isolated and closed pores, since these promote fatigue crack initiation and growth at the surface of the compacts [102], [103]. High-temperature sintering or liquid phase sintering enhances the densification by increment of 0.5-1.5% in case of

press and sinter route [9], [77]. The increased sintering temperature results in reduced stress concentration due to the rounding of pores. Reduction of surface oxides of Cr, Mn and Si becomes thermodynamically favored at elevated temperatures, where increasing temperatures shifts the reduction equilibrium to higher oxygen partial pressures. Formation of stronger inter-particle necks leads to enhanced densification during high-temperature sintering. The effect of the density significantly impacts on the physical, mechanical, and thermal properties, as illustrated in **Figure 14**.

In summary, the overall power-law relation to depict the role of density on property can according to Beiss et al. (8) be formulated as (ref):

$$\frac{P}{P_o} = \left(\frac{\rho}{\rho_o}\right)^m \qquad (1)$$

where P is the property of interest, P_o is the value for the pore-free material, ρ is density of the material, ρ_o is density of the pore-free material, and m is an exponent that takes on a specific value that depends on a particular property.

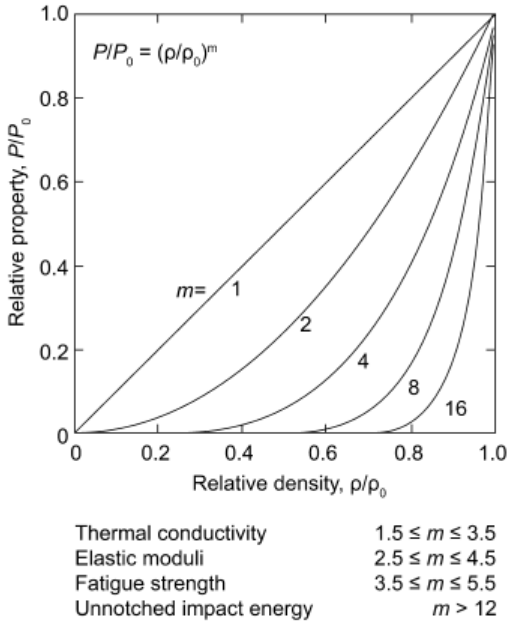

Figure 14. Density dependence of mechanical and physical properties of PM materials [8].

3.2 Microstructure for High-Performance Structural and Functional Components

PM steels from water-atomized and gas-atomized powder

Although there exist some applications of plain water-atomized iron powder, it is the utmost requirement to alloy the material that enables an enhancement in the mechanical properties of final part. Alloying is thus a necessary measure to ensure necessary thermal processability and hardenability. As described in Section 2.3, alloying

can be done in a few ways. Since few decades, Cr-alloyed PM steels have been developed for high performance applications. The Cr is pre-alloyed to the base powder in the atomization process due to its high affinity to oxidation [36], [58] and the Cr improves the hardenability of the sintered material, hence the achievable strength [78], [104]. Alloying elements such as Ni and Cu are admixed to the Cr-alloyed PM steel by diffusion bonding, owing to their low affinity to oxygen as this constitutes no risk for oxide control. Furthermore, since both elements have strong solution hardening effect, this approach prevents from reducing the compressibility of the material and promotes the hardenability. Hence, Cr-alloyed PM steels having Ni has inhomogeneous microstructure with nickel-rich regions besides the main steel microstructure. The Ni-rich regions could be both beneficial and detrimental to the mechanical properties [105]. Previous studies have reported that the reduction in inhomogeneity distribution of Ni in presence of Cr, with martensite and bainite being promoted which improves the mechanical strength [101], [106].

Many studies have shown that density and microstructure of the PM steels jointly influence their mechanical performance [6], [7], [107]. With the PM processing route, by tuning from the powder characteristics to the final component through choice of compaction and sintering strategies, tailored microstructure combined with increased sintered density are achievable, resulting in improved mechanical performance. Eventually, the microstructure obtained in PM steel relies on composition of the alloy material, sintering process and the cooling rate applied during sintering as well as the design of post-sintering heat treatment. Applying forced controlled cooling rate in the sintering run is termed sinter hardening and has been demonstrated for PM Steel with 3 wt.% Cr [108]. For grades with lower Cr-content of say 1.8 wt.%, these are most suited for post-sintering heat treatment and possibly case carburizing [46]. In essence, depending on the alloying route of powder grade mixtures, microstructures can vary further, for example for Ni-containing diffusion-alloyed PM steel, the heterogeneous microstructure is preserved as the interdiffusion of Ni and Fe is too limited at sintering to provide for complete homogenization. As a result, Ni-containing PM steel reveals different microconstituents such as martensite, bainite, pearlite, Ni-rich martensite and Ni-rich austenite in a material that exhibits combination of high strength without compromising on the toughness [108], [109], [110].

The PM tool steels made from gas-atomized powder exhibit the presence of strengthening phases resulting in desired microstructure after post-heat treatments to achieve superior mechanical properties. The superior hardness, remarkable fatigue and wear resistance of high-speed steels and high alloyed tool steels are achieved through a combination of microstructure and composition. Classically, these PM tool steels are produced by HIP of encapsulated and evacuated powder billets, following post-HIP machining and heat treatment (hardening and tempering) to realize final shape and microstructure. After hardening, these PM tool steels are primarily composed of martensite, a very hard but brittle phase formed during quenching. Tempering, the subsequent heat treatment, promotes the precipitation of secondary carbides within the martensite matrix. These hard, dispersed carbides further enhance hardness and provide

superior wear resistance [21], [111]. However, these inclusions at the surface of the compacts give rises to fatigue crack initiation and then eventually its propagation. Hence, high density of the material is desirable with complete removal of surface pores. To facilitate the manufacture of shaped components to near-net shape without encapsulated HIP and post-HIP machining, the studied novel route involving CIP, sintering and HIP is of interest.

Additive manufacturing

Many studies have been carried out on investigating the conductivity of pure copper related to impurities and relative density [112], [113], [114]. Thermal and electrical conductivities of pure copper increase with increase in density. In recent studies, the functional aspect of pure copper is dependent on its microstructure, such as grain boundaries and grain size [115], [116]. Low and high angle grain boundaries greatly impact material strength and conductivity. High angle grain boundaries inhibit the electron free path movement, resulting in lower electrical conductivity [113], [117]. Coarse grain specimen obtained higher electrical conductivity by 20% IACS, compared to that of fine grain specimen by 15% IACS [118]. However, finer grain sizes enhance the material strength due to the increased presence of boundaries that hinder dislocations movement [116], [118]. A critical challenge exists in optimizing pure copper for both high electrical conductivity and adequate mechanical strength. This approach involves careful tailoring of factors like grain size, overall microstructure and the inclusion of specific impurities.

3.3 Geometrical Characteristics for High-performance Structural and Functional Components

Fabrication of large components via uniaxial compaction is difficult when compared to CIP process, where components of 500 mm height and 200 mm diameter are possible to realise by isostatic compaction. In uniaxial compaction, the non-uniform distribution of density across the compact not only significantly hinders its green strength, but also negatively impacts dimensional accuracy and mechanical properties after subsequent sintering and heat treatment for such components [50]. There is limited research reported in the literature on fabricating complex geometries through CIP of metal powder. This gap is attributed to the challenges in designing suitable tooling, accurately predicting shrinkage during processing, and achieving tight dimensional tolerances [53]. In contrast to uniaxial compaction, CIP offers a significant advantage in terms of geometrical flexibility achievable in the final component, making it suitable for long-thin wall cylinders, parts with undercuts and three-dimensional curved geometries [52]. High performance gears fabricated through CIP, sintering and capsule-free HIP are shown in **Figure 15**.

Figure 15.(a) Cylindrical puck of high-performance PM steels fabricated through cold isostatic pressing (CIP), high temperature sintering (1250 °C) and capsule-free hot isostatic pressing (HIP) processes (b) gears machined from this puck.

Additive manufacturing technologies enable flexibility in manufacturing complex designs. Furthermore, there is plethora of literature available on achieving full densification of 316L stainless steel through powder bed fusion – laser beam (PBF -LB) [119], [120], [121]. Challenge arises to fabricate functional components of 316L where surface quality is a question which impacts the performance of the component. In recent years, there has been a high demand for manufacturing high-performance devices through AM process, to minimize the extensive post-processing steps. Similarly, achieving high density of pure copper using PBF-LB is a challenge due to its high reflectivity to the laser used. Hence, in this study, powder bed fusion – electron beam (PBF-EB) is used for manufacturing pure copper components for functional applications. Also, investigation of 316L components fabricated with fine features as prototype to explore feature control for applications such as waveguides, filters and antenna is also considered. Whereafter processing can be transferred to more conductive material. Likely, for pure copper, various melt strategies used in PBF-EB to manufacture dense components with high functionality are studied.

CHAPTER 4

Materials and Methods

This chapter provides a brief overview of the materials, processes and experimental techniques used in this thesis study and their respective background.

4.1 Materials and Processes

4.1.1 CIP Mould Fabrication

In order to create flexible mould for CIP, a novel approach involving the 3D-printing of moulds was developed applying the material extrusion technique fused deposition modelling (FDM). The flexible moulds were fabricated using Thermoplastic Polyurethane (TPU) filament in ZYXX+ FDM printer. The TPU as mould material was chosen to provide appropriate shore hardness for the CIP processing. Trails were made with different printed mould shapes in combination with different thicknesses. As can be seen below in **Figure 16**, conical, rectangular and screw shapes were fabricated.

As seen in **Figure 17**, CIP trials were made using these moulds filled with metal powder. The powder grades used were CrA-2Ni-0.3C and Vanadis 4E with powder sizes of <20µm. The CIP was done at 600 MPa on CrA-2Ni-0.3C using the QFP35L-600 machine at Quintus Technologies AB, Sweden and at 300 MPa on Vanadis 4E using Quintus Technologies at RISE AB, Sweden. For the Vanadis 4E, a special granulation process was done prior to CIP. Before CIP, the powder was filled in these moulds and placed it in a bag for evacuation. Later, this bag was placed in chamber and underwent CIP process using water as pressure medium. It is evident that intricate shapes could be CIP-processed using the flexible FDM printing.

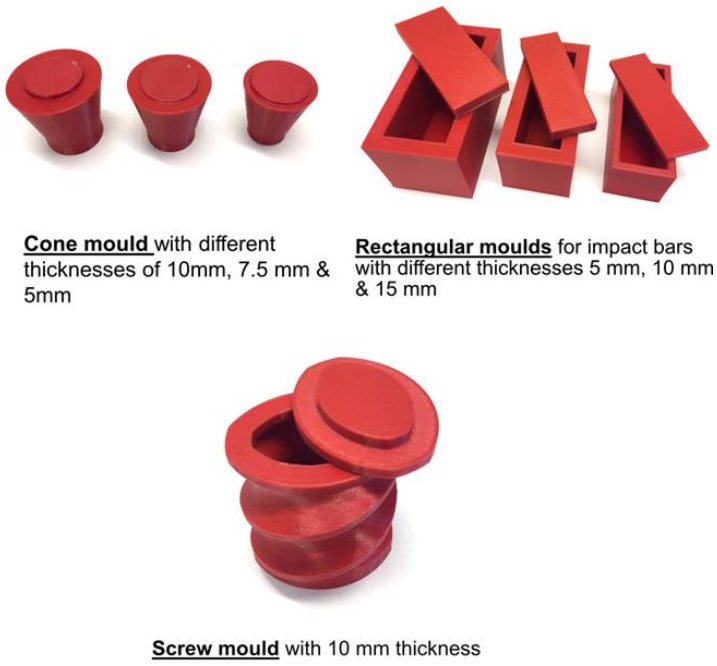

Figure 16. The 3D printed moulds are made from thermoplastic polyurethane filaments using ZYYX+ FDM printer.

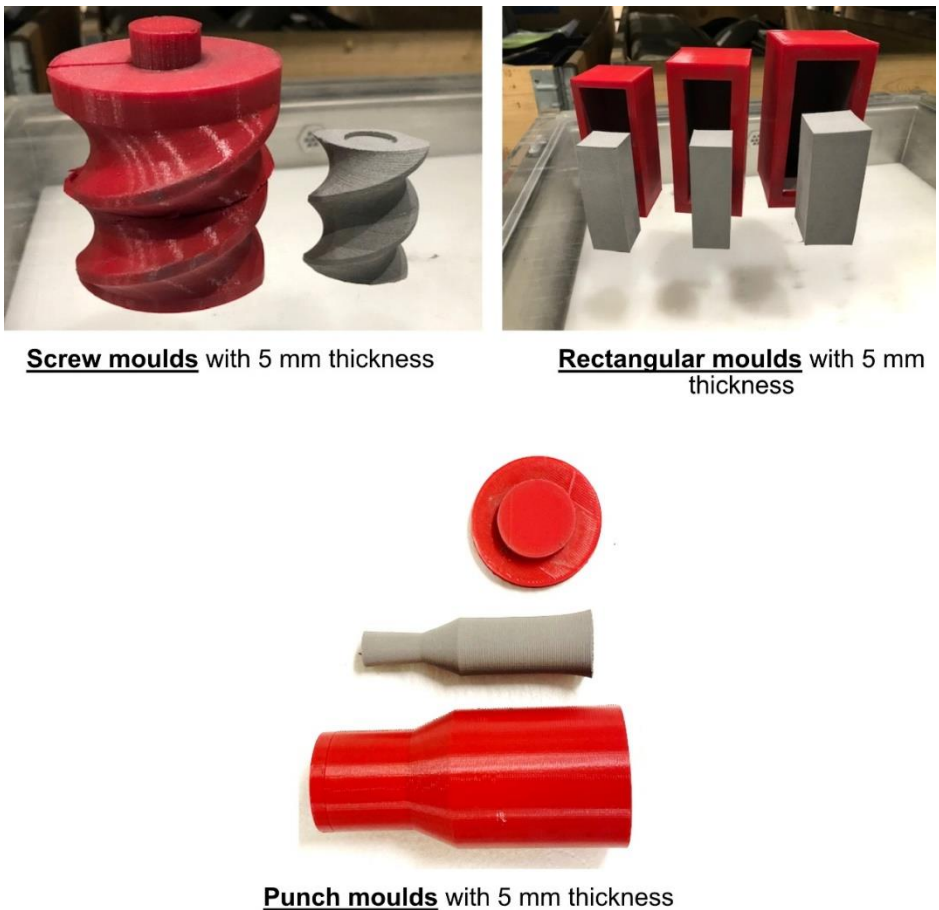

Figure 17. CIP process applied on complex flexible shapes.

4.1.2 Cold Isostatic Pressing (CIP), Sinter and Capsule-free HIP of Cr-alloyed steel

Water-atomized Cr-alloyed powder (known as CrA) admixed with 2 wt.% nickel and 0.3 wt.% UF-4 natural graphite from Höganäs AB was used. The addition of nickel was done by means of diffusion alloying method by Höganäs AB. The chemical composition of the powder grade including the added carbon is provided in **Table 1**.

Table 1. Composition of Cr-alloyed steel powder with admixed nickel and graphite in wt.%, C* = carbon in the form of graphite

Powder	Fe	Cr	Ni	C*	O	N	S
CrA-2Ni-0.3C	Bal.	1.8	2	0.3	0.15	0.007	0.002

An overview SEM image of the aforementioned powder grade termed CrA-2Ni-0.3C powder mix can be seen in **Figure 18** below.

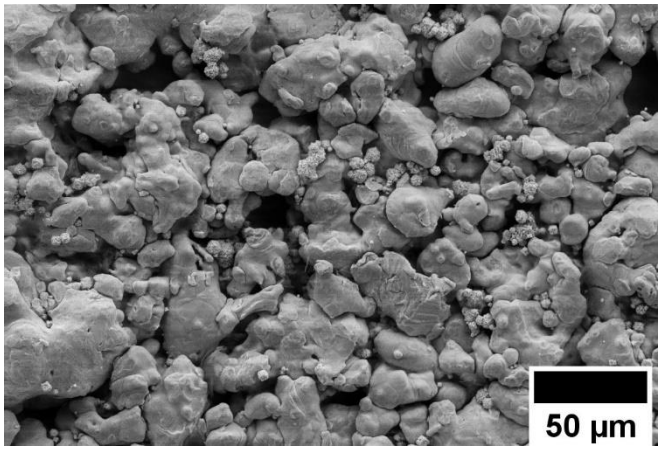

Figure 18. Overview of Cr-alloyed steel powder diffusion-bonded with 2 wt.%Ni and admixed with 0.3 wt.%C.

The CIP specimens of cylindrical shape were prepared by placing the powder samples in CIP moulds in vacuum sealed bags using water as pressure media. All the CIP specimens were produced using flexible rubber moulds of 27 mm height and 19 mm diameter in QFP35L-600 at Quintus Technologies AB, Sweden. The CIP pressures applied were 300 MPa, 450 MPa and 600 MPa, respectively, for 120 seconds of holding time per cycle. The sintering was performed in NETZSCH DIL 402C dilatometer at two different conditions: in $90N_2/10H_2$ atmosphere at 1120 °C and 1250 °C and in vacuum at 10^{-2} mbar at 1250 °C and 1350 °C, respectively. For both the conditions, heating rate of 10 °C/min and cooling rate of 30 °C/min were used with 60 min of holding time for the isothermal stage. Capsule-free HIP of the sintered specimens was carried out in QIH121 furnace at Quintus Technologies AB, Sweden using argon gas by applying pressure of 100 MPa at 1150 °C for 120 minutes. All the samples were normalized after HIP by heat treating to 960 °C in N_2

atmosphere for 60 min of holding time during the isothermal stage. This was done to compare the role of processing with respect to defect/pore content and eliminate the role of microstructure. For application purposes, the normalizing treatment is not a common approach, whereas rather there is an adjusted heat treatment for the application intended. A schematic diagram of the basic processing route is shown in **Figure 19**.

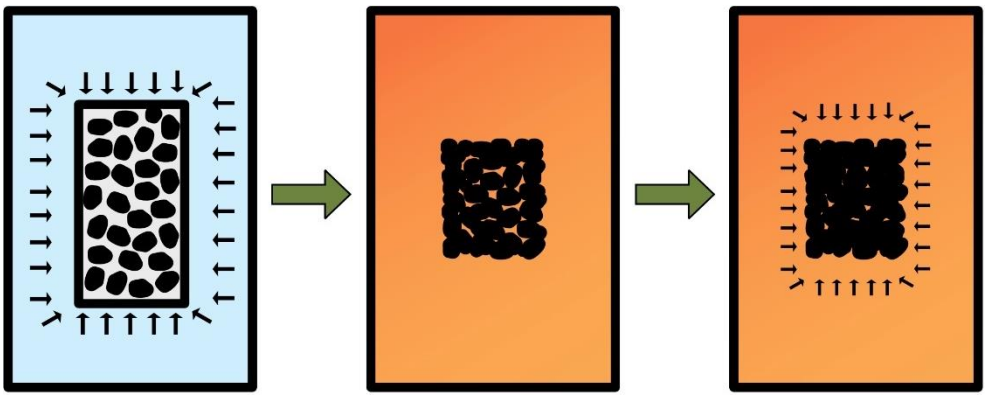

Figure 19. Schematics of procedure to obtain high density via cold isostatic pressing (CIP), sintering and capsule-free hot isostatic pressing (capsule-free HIP).

4.1.3 Compaction and Sintering Approach for Cr-alloyed steel – Role of Ni

To evaluate the effect of Ni addition, the water atomized CrA powder without and with 2 wt.% added Ni was processed by conventional uniaxial compaction followed by sintering. Also, 0.3 wt.% UF-4 natural graphite was admixed to the powder variants. Intralube® E lubricant was also applied, and compaction was done at Höganäs AB, Sweden. The chemical compositions of the variants studied are given in **Table 2**.

Table 2. Chemical compositions in wt.% of the powder variants without and with added Ni, C* = Carbon in the form of graphite

Materials	Cr	Ni	C*	O	Fe
CrA-0.3C	1.8	-	0.3	0.15	Bal.
CrA-2Ni-0.3C	1.8	2	0.3	0.15	Bal.

The compacts of the two powder grades were prepared by uniaxial pressing into cylindrical shape with dimensions of 10 mm height and 10 mm diameter, and in the form of Charpy impact bars with dimensions of 10 x 10 x 50 mm^3 according to ISO 5754. Compaction was done using pressure of 550 MPa to green density of 7.1 g/cm^3. After compaction, lubricant was removed by delubrication at 450 °C for 30 minutes in dry nitrogen atmosphere. The sintering runs were then performed at 1120 °C and 1250 °C in

a NETZSCH DIL 402C dilatometer in $90N_2/10H_2$ atmosphere for 60 minutes of holding time at isothermal stage. For both materials, heating rate of 10 °C/min and cooling rate of 30 °C/min were employed.

4.1.4 Granulation, Sintering and Capsule-free HIP of Gas-atomised Tool Steel Powder

Gas-atomized tool steel powder of grade Vanadis 4E with size distribution of <20 µm from Uddeholm AB was explored as prototype material for processing following the route of CIP, sintering and final capsule-free HIP. Chemical composition is given below in **Table 3**. To accomplish the aforementioned processing route, granulation of the spherically shaped powder to allow for CIP is a necessary must. Compressibility of the spherical powder, when having high hardness as in the case in question, is strongly restricted as there is no particle interlocking during compaction. Trials were done trying to compact this powder uniaxially, but this was not successful in obtaining any appropriate green strength. Hence, granules of the powder were prepared using freeze granulation technique as described in section 2.4. Mixes with varying content of Halt B-26 binder from 10 vol.% to 30 vol.% were prepared and the compaction with binder content of 25 vol% was shown to be enough functional.

Table 3. Nominal Composition in wt.% of gas-atomized tool steel powder (Vanadis 4E)

Powder	C	Si	Mn	Cr	Mo	V	Fe
Vanadis 4E	1.4	0.4	0.4	4.7	3.5	3.7	Bal.

The granules were pre-pressed uniaxially at 20 MPa to shape them into cylindrical form. These samples were then placed in a vacuum seal bag, before being CIP-processed at 300 MPa for 120 seconds per cycle in a laboratory cold isostatic press, Quintus Technologies at RISE AB, Sweden. All the CIP specimens produced were in dimensions of 10 mm in height and 10 mm diameter. Debinding of the CIP samples were done in a quartz tube furnace at 600 °C for 60 minutes in argon gas. The sintering trials were then performed in NETZSCH DIL 402C dilatometer at two different temperatures of 1150 °C, and 1200 °C in 100% N_2 atmosphere. The reason for selecting nitrogen as sintering atmosphere is that the nitrogen absorption into tool steel is expected to widen the sintering window and make liquid phase sintering possible and controllable. Heating rate of 10 °C/min and cooling rate of 30 °C/min were used with 60 min of holding time during isothermal stage for all the CIP samples. Later, Capsule-free HIP of the sintered specimens was carried out in QIH-48 furnace at Uddeholms AB, Sweden, using argon gas by applying pressure of 150 MPa at 1140 °C for 90 minutes. Furthermore, hardening on the capsule-free HIP-processed samples was carried out at 1100 °C for 30 min under vacuum, followed by rapid cooling at T8-5 ramp, in 100 s. Subsequently, tempering after capsule-free HIP samples was performed at 525 °C with 120 minutes of holding time for 3 times.

Similarly, gas-atomized powder grade of FeCrAl with a size distribution of 4-25 µm from Kanthal AB, Sweden was used for producing granules through freeze granulation method with 10 vol.% of PEG 6000 binder, followed by CIP at 350 MPa for 120 seconds per cycle in a laboratory cold isostatic press, Quintus Technologies at RISE AB, Sweden. Chemical composition is given below in **Table 4**. Debinding was carried out in an argon atmosphere at 600 °C and sintering trials were conducted in NETZSCH DIL 402C at different temperatures from 1250 °C to 1450 °C with an interval of 50 °C in hydrogen atmosphere. Heating rate of 10 °C/min and cooling rate of 30 °C were used with 60 min of holding time during isothermal stage for all the CIP samples. The CIP process yielded specimens with consistent geometry, each measuring 10 mm in height and 10 mm in diameter.

Table 4. *Nominal Composition in* wt.% *of gas-atomized FeCrAl powder (Kanthal)*

Powder	C	Si	Mn	Cr	Al	O	Fe
Nom. composition						0.02	Bal.
Min	-	-	-	19.0	4.5		
Max	0.08	0.7	0.4	23.5	5.5		

4.1.5 PBF-LB of 316L and PBF-EB of Pure Copper

Gas atomized 316L stainless steel was used for PBF-LB process. Geometries of artefact components and functional waveguide test objects as shown in **Figure 20** were fabricated with 316L material.

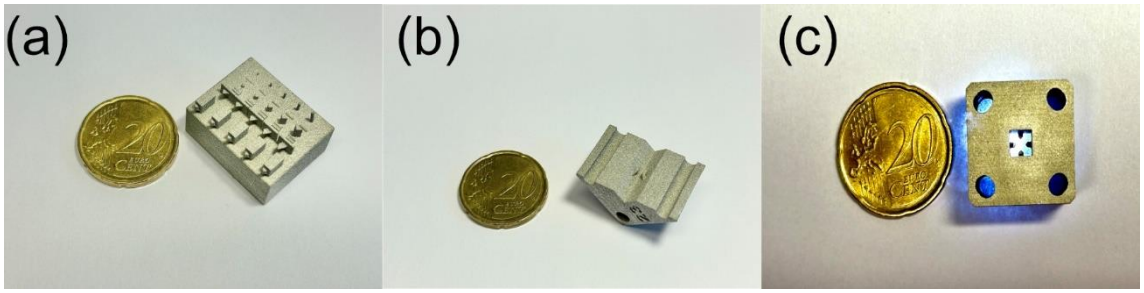

Figure 20. Functional samples fabricated using PBF-LB of 316L stainless steel; (a) artefact components, (b) cut piece wave guide, and (c) quad-ridge test resonator with four arrowheads.

Pure copper powder (purity 99.95%) was used to fabricate components using different melt strategies such as hatch and point melt during PBF-EB process on Q10 frame equipped with a V2.1 Spectra H EBU (Collibrium Additive, Sweden). The spherical powder was gas atomized with a particle size distribution of D10 is 53.1 µm, D50 is 68.6 µm, and D90 is 91.9 µm provided by TLS/Eckart GmbH (Germany).

4.2 Analytical Techniques

This section summarizes the analysis employed in this thesis study. If not otherwise stated, the analyses were employed at the Department of Industrial and Materials Science, Chalmers University of Technology, by the author.

4.2.1 Dilatometry (DIL)

The dimensional change of a specimen is accurately measured by dilatometry as a function of temperature and time. For heating cycle this means the total effect of linear sintering shrinkage and thermal expansion as well as contraction/expansion owing to phase changes. The instrument used for the dilatometer experiments as shown in **Figure 21** is a DIL 402C from NETZSCH (NETZSCH-Gerätebau GmbH, Germany) equipped with W-Re thermocouple for inert or reducing atmosphere and S-thermocouple for vacuum. The horizontal push rod dilatometer is connected to displacement transducer, which converts the linear displacement into measurement signals with a high resolution of up to 0.125 nm or 1.25 nm, depending on the range of measurement. For analysis, the specimen is placed in alumina holder and the horizontal push rod is positioned directly against the holder with a minimum force of 25 cN. The dilatometer chamber is connected to the rotary and turbo pumps in sequence to perform sintering at vacuum down 10^{-4} mbar. The instrument is evacuated and flushed with argon gas up to three times before each measurement to reduce air residues.

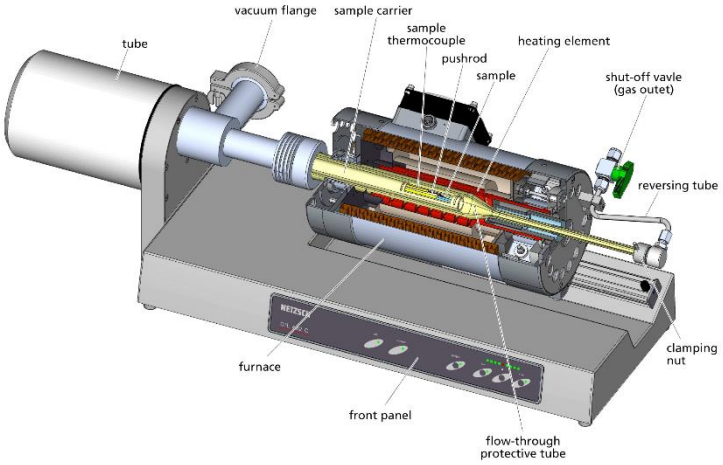

Figure 2: DIL 402 C measuring unit (cross - section)

Figure 21. Schematic view of NETZSCH DIL 402C dilatometer, (With permission).

4.2.2 Thermogravimetry (TG)

Thermogravimetry (TG) is a thermoanalytical technique used for monitoring change in mass of a specimen as a function of temperature. During TG analysis, the changes in the specimen mass are recorded as the specimen is heated/cooled to specific temperatures with controlled heating and cooling rates. The instrument used for thermogravimetric experiments as shown in **Figure 22** is a simultaneous TGA/DTA/DSC analyser STA 449 F1 Jupiter from Netzsch (NETZSCH-Gerätebau GmbH, Germany). Before starting the experiment, specimen of mass of about 2000 mg is collected into an alumina crucible, which is placed inside the instrument. Like mentioned for DIL 402C, the TG instrument can be evacuated using turbo pump backed with rotary pump and the chamber is usually

flushed with argon gas up to three times before each measurement to reduce air residues before setting the atmospheric conditions for the experiment.

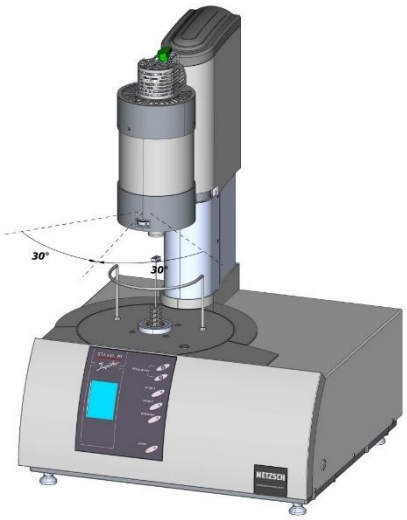

Figure 22. Schematic illustration of STA 449 F1 Jupiter from Netzsch, (With permission).

4.2.3 Density Measurements

Archimedes water displacement technique according to ASTM B328 was used for measuring density of the samples. The measurements were done on green (after CIP), sintered and HIP samples. The weight of the sample was measured in air, then followed by measuring weight in water using a setup balance of 0.0001 g accuracy. The density of the sample is calculated according to:

$$\text{Density, } \rho = \frac{W_a \, X \, \rho_w}{W_a - W_w} \text{ (in g/cm}^3\text{)} \qquad (2)$$

Where W_a and W_w are the weights of the samples in air and water measured in grams, $\boldsymbol{\rho_w}$ is the density of the water (1 g/cm^3). To seal the open pores, samples were impregnated with paraffin wax before the measurements.

4.2.4 Helium Gas Pycnometry

The helium gas pycnometer is operated on the principle of Boyle's law through which true density of the sample is measured. Helium is most widely used because of its smaller molecular size, which means that the helium molecule can penetrate through almost every pore down to atomic scale, considering its ideal gas behaviour as well. The AccuPycII 1340 He-pycnometer instrument was used at Höganäs AB. The true density measured using this technique provides the closed porosity of the samples.

4.2.5 Light Optical Microscopy

Light optical microscopy (LOM) is a technique in which visible light is used as a source, illuminated on the surface of a sample for topography, phase composition or feature

contrast. The instrument used to capture the LOM images is the ZEISS Axioscope 7 equipped with digital camera for further analysis. Samples for investigation were prepared by mounting with a conductive resin, PolyFast from Struers, using hot mounting machine from Citropress-20, Struers. Grinding and polishing of these samples were done on Struers TegraPol-31 machine. The grinding was done using SiC paper of 320-grit, 500-grit, 1000-grit, 4000-grit in sequence and polishing was done using suspended diamond solutions of 9 µm, 3 µm and 1 µm in steps. Mirror-like surfaces are in this way achieved after the final polishing step. Etching of these samples was done using 2% Nital to reveal the microstructure. However, porosity analysis was performed on polished samples before etching.

4.2.6 Scanning Electron Microscopy

Scanning electron microscopy (SEM) was used for high spatial resolution imaging. The high magnification provides information about surface topography and microstructural features. The fundamental principle of SEM involves directing the electron beam from source onto the surface of the sample. Thus, different types of radiation are generated such as Auger electrons (AE), secondary electrons (SE), back-scattered electrons (BSE) and X-rays. In this study secondary electron (SE) imaging was used for microstructural features and surface topography of the powder and bulk samples, chemical analysis, and mapping. The work presented in this thesis has been performed using a Gemini SEM 450 Zeiss instrument equipped with X-ray energy dispersive spectroscopy (EDS) employed for chemical analysis. Electron back scattered diffraction (EBSD) was performed to investigate the phase composition and grain boundaries with a Nordlys II detector (Oxford Instruments).

4.2.7 X-Ray Diffraction (XRD)

X-ray diffraction (XRD) is used to determine phases by investigating the crystal structure. Bragg's law as mentioned below is used to detect the patterns of the peak intensity. In this thesis, a Bruker D8 discovery instrument is used using Cu-tube as a radiation source emitting an X-ray radiation CuKα(λ=1.54060 Å), and the working voltage was set to 40kV with a current of 40 mA.

$$n\lambda = 2 * d * \sin\theta \quad (3)$$

4.2.8 Chemical Analysis

Chemical analysis was performed at Höganäs AB for bulk oxygen and carbon concentration of powder, sintered samples and HIP samples of the Cr-alloyed materials using LECO TC-600 and LECO CS-844 instruments. For oxygen analysis, the sample was heated in a graphite crucible in helium gas, during which interaction between the oxygen and carbon from the crucible takes place resulting in release of CO and CO_2. This escaped gas mixture is detected by the IR detectors, which indirectly then measures the oxygen content. The carbon analysis was performed in an induction furnace with oxygen

flow where sample is combusted. The carbon from the sample reacts then with the oxygen forming CO and CO_2 gas, which is again detected by the IR detectors to determine the carbon content.

Chemical analysis was performed for bulk carbon and sulphur content of sintered and HIP samples of PM tool steel using LECO CS-600 instrument through combustion process at Uddeholms AB. The oxygen and nitrogen levels were determined using LECO ONH836 through melt extraction process.

Chemical analysis for light elements C, S, N and O was done via external accredited laboratory ISO 17025:2017 using LECO CS600 for C, LECO CS844 for S and LECO ON836 for O and N. The methods are based on ASTM E1019-18 for inert gas fusion techniques.

4.2.9 Hardness Testing

Hardness of a material is defined as the measure of materials resistance to plastic deformation on indentation. In this thesis study, Vickers hardness technique was used. This technique uses a diamond shaped indenter with an angle of 136° between the faces and the tests were employed on sintered and HIP samples. A pre-defined load (L) is applied on the sample and the average diagonals lengths of the indentation on the sample are measured. According to the ASTM E384-17 standard, hardness value is calculated as follows:

$$HV = 1.8544 \frac{L}{d^2} \quad (4)$$

where HV is the Vickers hardness in HV, L is the load applied in kgf and d is the average diagonal length of the indentations, in mm. The equipment used was Struers Durascan-70 G5 instrument for both Cr-alloyed steel and tool steel samples.

4.2.10 Impact Testing

Impact testing was done on IE bars prepared according to ISO 5754 using Instron PW 30 impact testing machine to evaluate impact energy values. These analyses were performed on 5 samples for each condition at Höganäs AB for Cr-alloyed steel samples.

4.2.11 Thermal Conductivity

Thermal diffusivity of pure copper was measured using laser flash analysis 447 (LFA) instrument according to ASTM E1461-13 standard, and later conductivity was calculated according to equation 4 below. All samples were prepared according to the standard dimensions required for sample holder with dimensions of 8x8 mm^2 and thickness of 1.5 mm.

$$\lambda = \alpha \, C_p \, \rho \quad (5)$$

Where α is thermal diffusivity, λ is thermal conductivity, ρ is density of the material and C_p is specific heat at constant pressure.

4.2.12 Electrical Conductivity

Electrical conductivity measurements were carried out according to DIN 50994 standard on all copper samples after process optimization. 10 measurements were done on each sample.

4.2.13 RF Frequency measurements

The quad-ridge (QR) test objects were used for functional testing at Ericsson AB, Sweden, to measure the resonance frequency and Q-value (quality factor the quality factor, or 2p times the stored energy vs energy dissipated per cycle which is inversely proportional to the width of the curve's peak).

4.2.14 Thermodynamic calculations

Thermodynamic calculations were performed using Thermo-Calc, a commercial CALPHAD (CALculation of PHAse Diagram) software using TCFE13 database for V4E tool steel and FeCrAl. These thermodynamic calculations are used to identify the melting temperature and influence of nitrogen on V4E tool steel, melting temperature and phase identification of FeCrAl. JMatPro software (Version 12.4) with general steel database was used on V4E tool steel and FeCrAl for phase identification and phase evolution predictions as well.

CHAPTER 5

Results

This section summarizes the results from the appended papers.

- Paper I is focused on the densification behaviour of PM steel made from water-atomized powder containing 1.8 wt.% Cr through the CIP→Sinter→Capsule-free HIP route. Analysis of the sintering behaviour for different sintering atmospheres and temperatures was therefore investigated.
- Paper II is extended to address the novel alternative processing route for the Cr-alloyed PM steel when sintering after CIP consolidation directly in in HIP furnace in combination with proceeding capsule-free HIP. Impact of this novel consolidation approach on densification, microstructure control and properties are studied.
- As alloying with Ni is crucial for the microstructure control for the aforementioned Cr-alloyed PM-steel, the role of Ni on sintering behaviour is further addressed in Paper III.
- In Papers IV and V, work focuses on densification behaviour of gas-atomized cold work PM tool steel and FeCrAl powder, through freeze granulation (FZ) technique, high temperature and liquid phase assisted sintering and capsule-free HIP.
- Paper VI is focused on investigation of geometrical tolerance control of 316L stainless steel fabricated through powder bed fusion – laser beam (PBF-LB).
- In Paper VII, pure copper is produced through powder bed fusion – electron beam (PBF-EB) using different melt strategies to investigate the impact of different melting strategies on density, microstructure, thermal and electrical properties.

5.1 Densification of Water Atomized Cr-alloy Steel Powder (Papers I, II)

The objective of the paper I was to depict the influence of processing parameters on the densification behaviour of Cr-alloyed steel powder depending on processing route. Specifically, the research is focused on the impact of different cold isostatic pressing (CIP) pressures namely 300 MPa, 450 MPa and 600 MPa, followed by sintering in $90N_2/10H_2$ atmosphere and vacuum (10^{-2} mbar) on the densification at varying temperatures. **Figure 23** represents the correlation between relative density as a function of applied CIP pressure and sintering temperature. Green density after CIP was

increased to 7.2 g/cm^3 with the increase in isostatic pressure to 600 MPa owing to deformation and packing of the irregularly shaped water-atomized metal particles. In **Figure 23(a)-(b)**, results for the sintering at 1250 °C in 90N_2/10H_2 and vacuum (10^{-2} mbar) demonstrate the potential in achieving almost closed porosity. A critical finding is the almost complete elimination of open porosity in samples subjected to CIP at 600 MPa for both sintering routes at 1250 °C. This enabled subsequent capsule-free HIP in argon gas after sintering to reach full density. Sintering in vacuum at 1350 °C resulted in a significant reduction of surface porosity, reaching 93% of theoretical density.

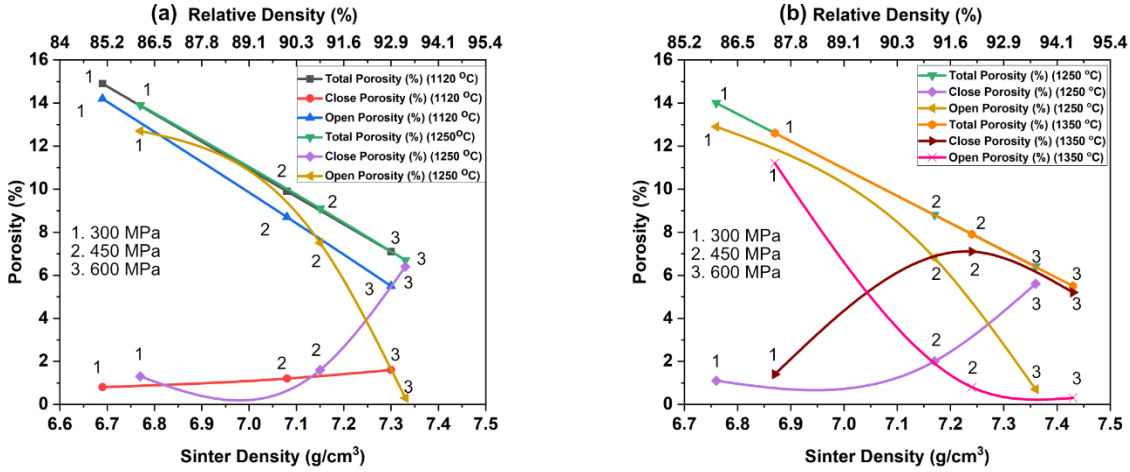

Figure 23. Open and closed porosities as a function of sintered density for sintering in (a) 90N_2+10H_2 and (b) vacuum (10^{-2} mbar) (Paper I) [77].

Figure 24 illustrates the density values of the samples after sintering and capsule-free HIP process. Density values after capsule-free HIP for samples cold isostatically pressed at 300 MPa are not considered owing to the presence of open porosity as seen in **Figure 24(a)**. The results in **Figure 24(a)** show that densification varies with increase in CIP pressure after sintering as well as after capsule-free HIP. Density values increased with increase in sintering temperature from 1120 °C to 1250 °C either when sintering in 90N_2/10H_2 or in vacuum at 10^{-2} mbar at 1250 °C and at 1350 °C. Based on the results presented in Paper I, it is concluded that density levels attained were sufficient to induce substantial surface densification, thereby facilitating the subsequent application of capsule-free HIP. Similar density of 7.82 g/cm^3 is achieved for samples subjected to capsule-free HIP following sintering at 1250 °C in 90N_2/10H_2 and in vacuum (10^{-2} mbar). Density of 7.84 g/cm^3 is achieved after sintering at 1350 °C in vacuum (10^{-2} mbar), followed by capsule-free HIP. **Figure 24(b)** illustrates the results from Paper II, which explores the elimination of separate sintering stage. Instead, the sintering is done in HIP furnace at 0.5 mbar vacuum followed by capsule-free HIP at 1150 °C. The density of 7.52 g/cm^3 was achieved when sintering at 1150 °C in the HIP furnace followed by capsule-free HIP, whereas a density of 7.84 g/cm^3 was obtained after sintering at 1250 °C in the HIP furnace and subsequent capsule-free HIP at 1150 °C. The latter density value indicates the attainment of full or near full densification through a two-stage process in a HIP furnace without any preceding sintering.

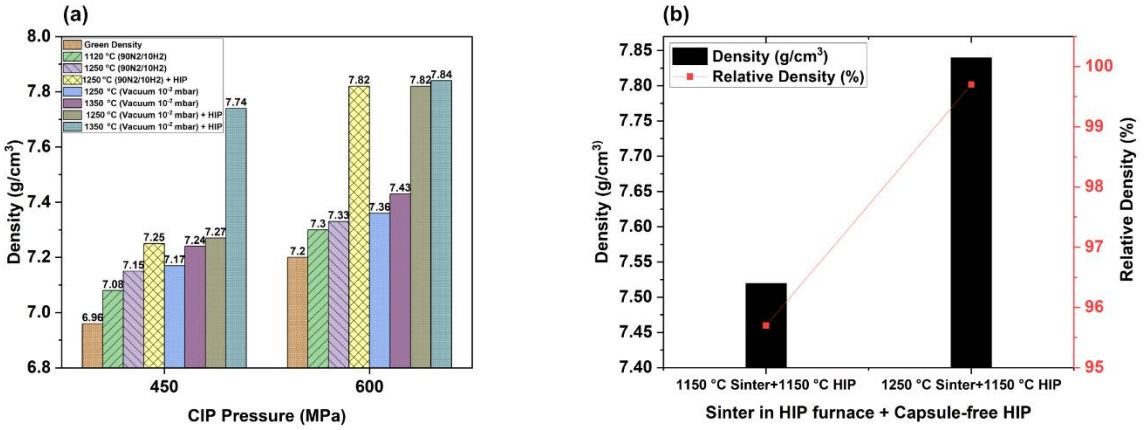

Figure 24. Archimedes density measurements of CrA-2Ni-0.3C after (a) CIP+Sinter+Capsule-free HIP (Paper I) (b) CIP+Sinter in HIP+Capsule-free HIP (Paper I and II) [77], [122].

5.2 Effect of Admixed Nickel on Densification of Water-atomized Cr Alloy Steel Powder (Paper III)

Nickel is a key element to achieve heat treatment capabilities of sintered steel. There is alot of interest to find out the role of nickel in more detail during the sintering. Hence, paper III was aimed at investigating the influence of nickel additions on the shrinkage behaviour of Cr-alloyed steel powder (CrA) with 0.3 wt.% added graphite. The impact of sintering results on selected mechanical properties was also addressed. Sintering experiments were conducted with specimens of both CrA-0.3C and CrA-2Ni-0.3C variants, uniaxially compacted to 7.1 g/cm3. The sintering was performed at 1120 °C and 1250 °C in $90N_2/10H_2$ atmosphere. Density values for these variants are shown in **Table 5**. Both CrA-0.3C and CrA-2Ni-0.3C variants exhibited an increase in density as sintering temperature increased. However, density was increased with the addition of admixed nickel, which activated the early formation of sinter neck bridges between the metal particles during the heating stage. This has then shown to have an impact on the overall shrinkage behaviour during sintering as evidenced from **Table 6**. Clearly, presence of admixed Ni, most probably related to the fine Ni particle size is supposed to be contributors to this fact. Therefore, the addition of Ni can be expected to enhance the required surface densification to facilitate subsequent capsule-free HIP.

Table 5. Archimedes density measurements of Cr pre-alloyed PM steels

Material	1120 °C	1250 °C
CrA-0.3C	7.16±0.04	7.22±0.01
CrA-2Ni-0.3C	7.23±0.01	7.28±0.01

The total dimensional changes are displayed in **Table 6**. The material containing Ni exhibited a higher percentage of dimensional change. This trend was observed at both

the lower and higher sintering temperatures of 1150 °C and 1250 °C, respectively. Clearly, the effect of Ni is as said related to the onset of sinter necks early on during the heating stage of the sintering. The material containing nickel exhibited the highest shrinkage, reaching a value of 0.45±0.01%. Material without nickel revealed the lowest shrinkage of 0.3±0.01% at the lower sintering temperature of 1120 °C.

Table 6. Total dimensional change for CrA-0.3C samples with and without nickel additions sintered at 1120 °C and 1250 °C

Materials	Sintering temperature (°C)	Dimensional change (%) (DIL)
CrA-0.3C	1120	-0.3±0.01
CrA-0.3C	1250	-0.41±0.02
CrA-2Ni-0.3C	1120	-0.42±0.01
CrA-2Ni-0.3C	1250	-0.45±0.01

5.3 Densification of Gas-Atomized Powder of Cold Work PM Tool Steel and FeCrAl Steel (Papers IV and V)

These investigations Papers IV and V) were aimed to exploit possibilities for enhanced densification of the gas-atomized powder of cold work PM tool steel and FeCrAl steel utilizing the freeze granulation (FG) technique for powder feedstock fabrication, followed by CIP, high temperature sintering and potential capsule-free HIP.

Cold Work Tool Steel

Freeze granulation process on gas-atomized tool steel powder of grade Vanadis 4E with size distribution of <20 µm was explored. These granules were CIP processed at 300 MPa, followed by sintering in nitrogen atmosphere. **Figure 25** presents the microstructure of samples sintered at 1150 °C and 1200 °C, followed by capsule-free HIP, hardening and tempering, as observed in unetched cross-sectional views. **Figure 25(a)** clearly illustrates a substantial amount of porosity in samples involving sintering at 1150 ·C, in contrast to the significantly reduced porosity observed in those involving sintering at 1200 °C, as depicted in **Figure 25(b)**. Notably both samples exhibited almost no pores following capsule-free HIP, hardening, and tempering, as evidenced in **Figure 25(c)-(d).** In comparison to the sample sintered at 1150 °C (**Figure (25(c)**), the sample sintered at 1200 °C exhibits a smoother surface (**Figure 25(d)**), confirming the findings in Paper IV regarding an adequate sintering process. These findings validate the density measurements obtained by the Archimedes method, as presented in Paper IV (Figure 4). Consequently, **Figure 25** provides evidence of the sintered density values determined for those samples after sintering at 1150 °C and 1200 °C, followed by subsequent capsule-free HIP, hardening and tempering.

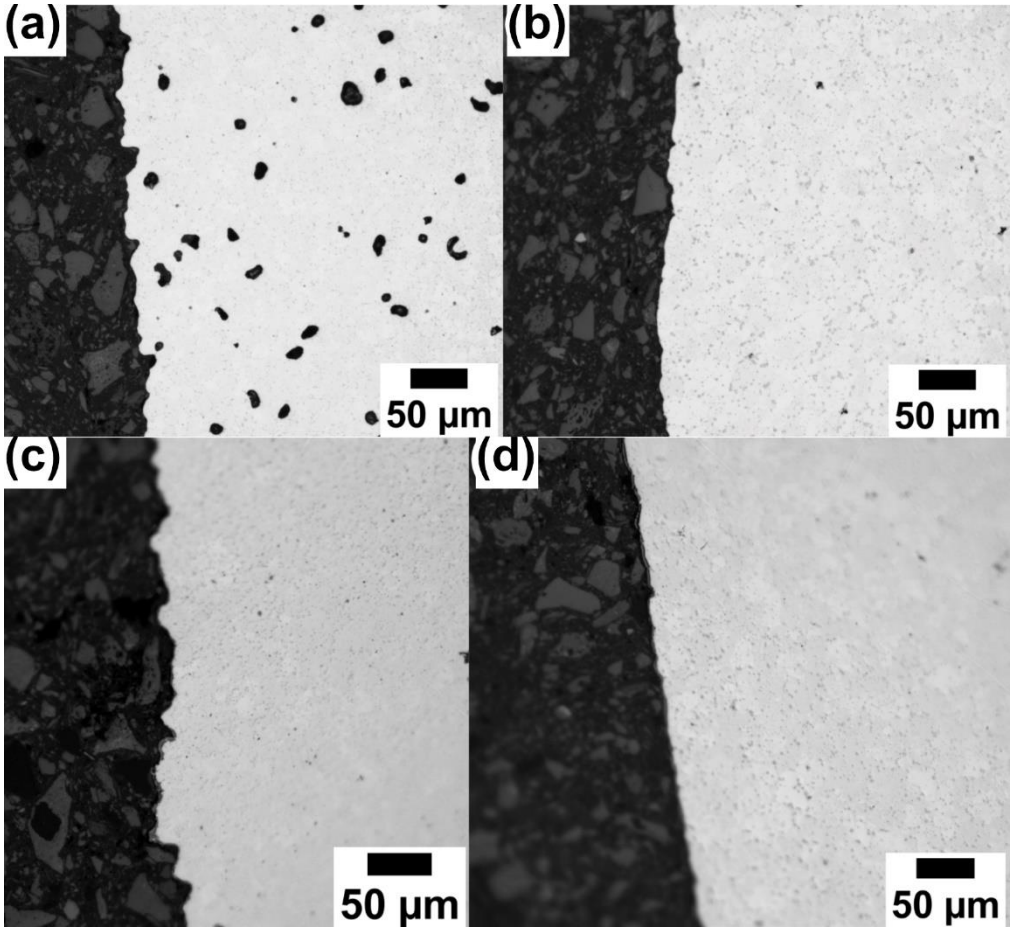

Figure 25. Optical micrographs of V4E material after sintering at (a) 1150 °C, and (b) 1200 °C, (c) sintering at 1150 °C followed by capsule-free HIP, hardening and tempering (d) sintering at 1200 °C followed by capsule-free HIP, hardening and tempering (Paper IV).

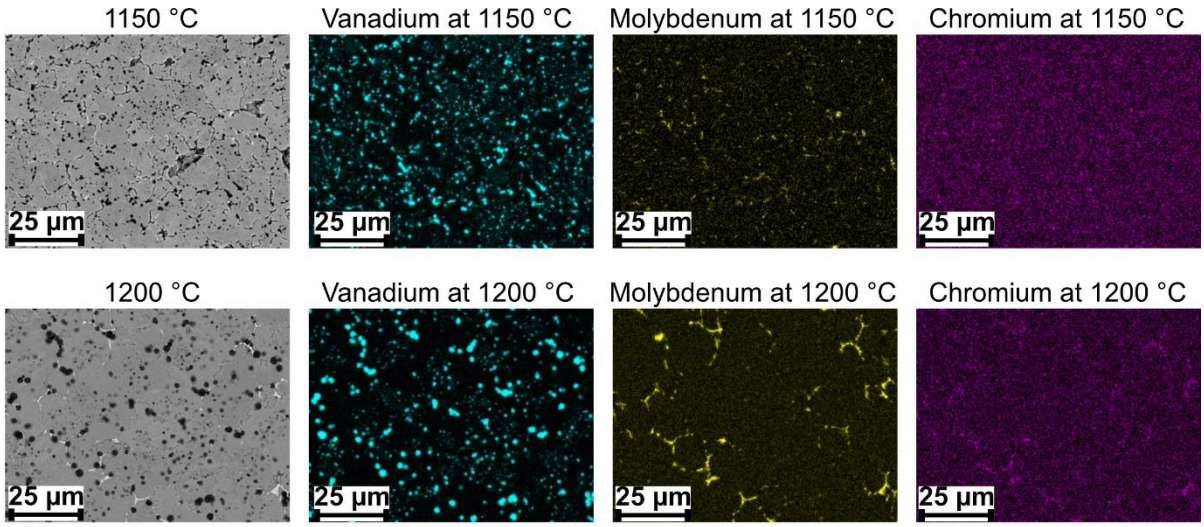

Figure 26. SEM images and EDS mapping of V4E material after sintering at 1150 °C (top row), and 1200 °C (bottom row) Paper IV.

Energy dispersive X-ray spectroscopy (EDS) mapping, as shown in **Figure 26**, revealed the presence of vanadium and molybdenum-containing precipitates within the sintered samples. For samples sintered at both the temperatures of 1150 °C and 1200 °C,

vanadium is predominantly located within the presumed MX precipitates, while molybdenum and chromium are most probably concentrated in carbide precipitates. The vanadium-rich precipitates involve two distinct MX precipitates size groups, larger precipitates preferentially located at the grain boundaries and smaller precipitates dispersed within the grains. Carbide precipitates exhibited a preferential distribution at the grain boundaries. **Table 7** represents the measured hardness values for samples after sintering as well after following capsule-free HIP, hardening and tempering. The hardness values measured for samples sintered at 1150 °C and 1200 °C were 335±7 HV10 and 444±14 HV10, respectively. The observed difference in hardness is attributed to the lower porosity evident in the former samples, as evident from **Figure 25(a)**. After subsequent capsule-free HIP and tempering, hardness values of 519±14 HV10 and 457±11 HV10 were determined for samples initially sintered at 1150 °C and 1200 °C, respectively. Attributing both samples to having achieved near full density, the observed hardness difference represents microstructural differences.

Table 7. Apparent hardness measurements of samples after sintering at 1150 °C and 1200 °C and after following capsule-free HIP, hardening and tempering

Sample	Apparent Hardness Measurement (HV10)	
	After Sintering	**After Capsule-free HIP + Tempering**
1150 °C	335±7	519±14
1200 °C	444±14	457±11

FeCrAl

Table 8 presents the results of Archimedes and geometrical density measurements performed on FeCrAl samples sintered at the final holding temperatures of 1250 °C, 1300 °C , 1350 °C, 1400 °C and 1450 °C in hydrogen atmosphere for 60 min, respectively. The relative density reached minimum of 99% for samples sintered at both 1400 °C and 1450 °C, with the latter achieving a relative density of 99.6%, considering 7.15 g/cm^3 as theoretical density. Notably, both Archimedes method and the geometrical density assessment give comparable and consistent results.

Table 8. Sintered densities and corresponding relative densities obtained for different sintering temperatures

Sintering temperature (°C)	Archimedes Density		Geometrical Density	
	g/cm3	**Rel. Den (%)**	**g/cm3**	**Rel. Den (%)**
1250	5.85±0.05	81.8±0.7	5.83±0.03	81.6±0.5
1300	6.35±0.18	88.9±2.5	6.38±0.17	94.97±0.14
1350	6.87±0.05	96.1±0.7	6.79±0.01	94.97±0.14
1400	7.08±0.01	99.0±0.1	6.99±0.11	97.76±1.48
1450	7.14±0.04	99.6±0.3	7.11±0.03	99.44±0.46

The feasibility of applying capsule-free HIP is indicated by the data in **Table 8** to samples sintered at 1350 °C. This is because when the total porosity levels are below 5-6%, the

predominant pores are mostly closed ones. Furthermore, sintering at 1400 °C is expected to yield near full density, eliminating the necessity for subsequent post-sintering HIP.

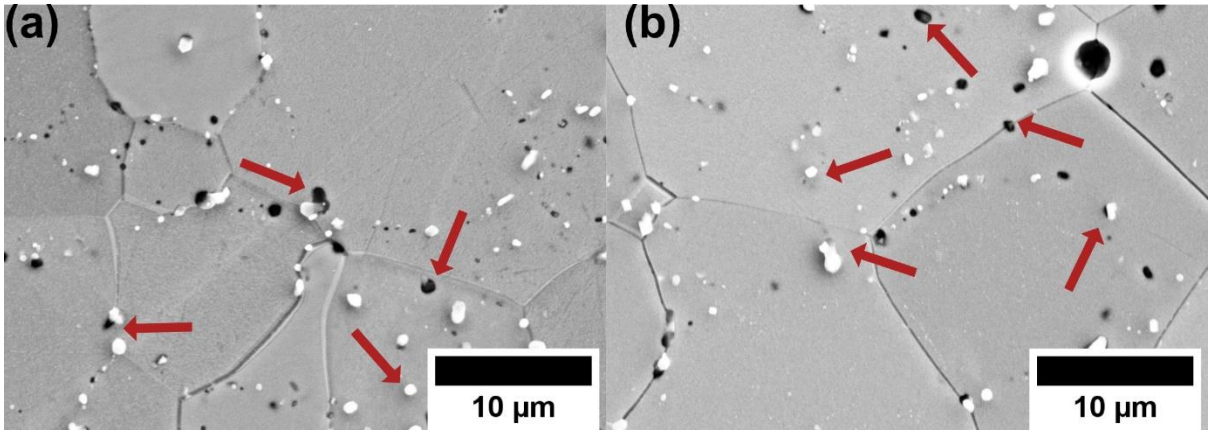

Figure 27. SEM imaging of cross-sections of samples sintered at 1400 °C (a) and 1450 °C. Red arrows indicate oxide inclusions in the specimens (Paper V).

Microstructural analysis as shown in **Figure 27** reveals a ferrite matrix structure in samples sintered 1400 °C and 1450 °C, accompanied by the presence of inclusions, characterized by a distinct whitish and darkish contrast. The EDS-analyses confirmed that all inclusions are Al-rich and O-rich, supposedly Al-oxide. The inclusions are observed to be located both at grain boundaries and within the grains, suggesting a degree of grain boundary pinning. This study revealed that higher sintering temperatures induce grain growth and detachment of grain boundaries from precipitates, although the grain size is not confirmed quantitatively. Thermodynamic simulations by JMatPro suggest that the at least at the higher temperature of 1450 °C, liquid phase assisted could be possible driven by residual carbon level from the binder used when freeze-granulating the powder. Also, the JMatPro confirmed that the theoretical composition of the Al-oxide is Al_2O_3 without any other alloying element present.

5.4 Precision Manufacturing of 316L for Functional Applications using PBF-LB (Paper VI)

Metal additive manufacturing is usually considered as a mean of creating structural parts. In Paper VI, the scope has therefore been to explore how metal additive manufacturing can be used for fabricating precision parts for functional applications. As a prototype material gas-atomized 316L powder has been used and printing was done by means of PBF-LB. The test prototypes were specially designed samples of interest to depict performance for wave guide components. Next step would be to shift to PBL-LB printing of Cu. However, this is outside the scope of this thesis study.

Figure 28 presents SEM images and dimensional measurements of arrows from half-part and full-part test resonators fabricated using PBF-LB. A total of 36 half-cut samples and 18 test resonators were fabricated. To comprehensively analyze the process, a representative subset of samples from different locations on a build plate, ranging from bottom left (1) and middle (5) and top right (9) locations, were selected for investigation.

Comparative analysis of the images in **Figure 28** revealed consistent similarities between left and right arrows within both the half part and test resonator across all the samples. A notable difference between the half-cut and test resonator samples lies in the impact of surrounding powder sintered on the arrow surfaces, which resulted in increased surface roughness for the former.

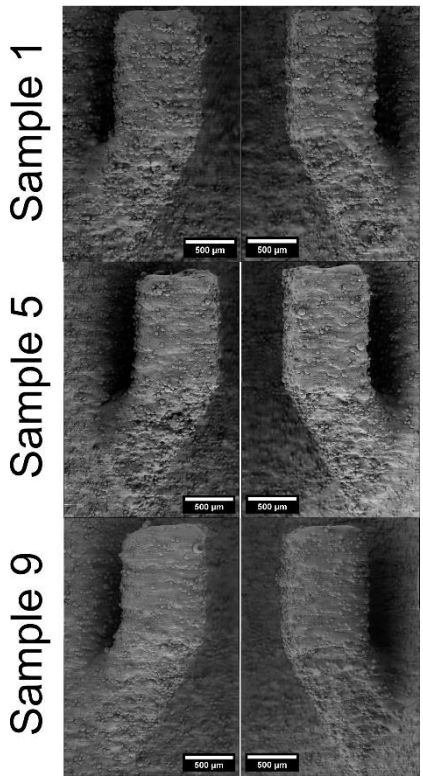

Figure 28. (a) SEM images of arrows from half-cut component (left vertical) and test resonator (right vertical)

As illustrated in **Figure 29,** the measured width of the half-cut components consistently exceeded the nominal value of 770 µm. While this nominal deviation is substantial, the degree of part-to-part variation is minimal. Part-to part variation in the angle measurement for the test resonator samples was also minimal, with all values exhibiting close proximity to the nominal value of 60 degrees. Hence, deviation in half-cut components likely stems from increased recoater movement while spreading the powder layer during the printing process, leading to compromised down-skin quality of the angular structure. However, sample 5 exhibited dimensional consistency with nominal values for both width and angle in the test resonator. Resonance frequencies measured were within the range from 28.8 GHz to 29.1 GHz, close to nominal value of 27.9 GHz predicted for 316L.

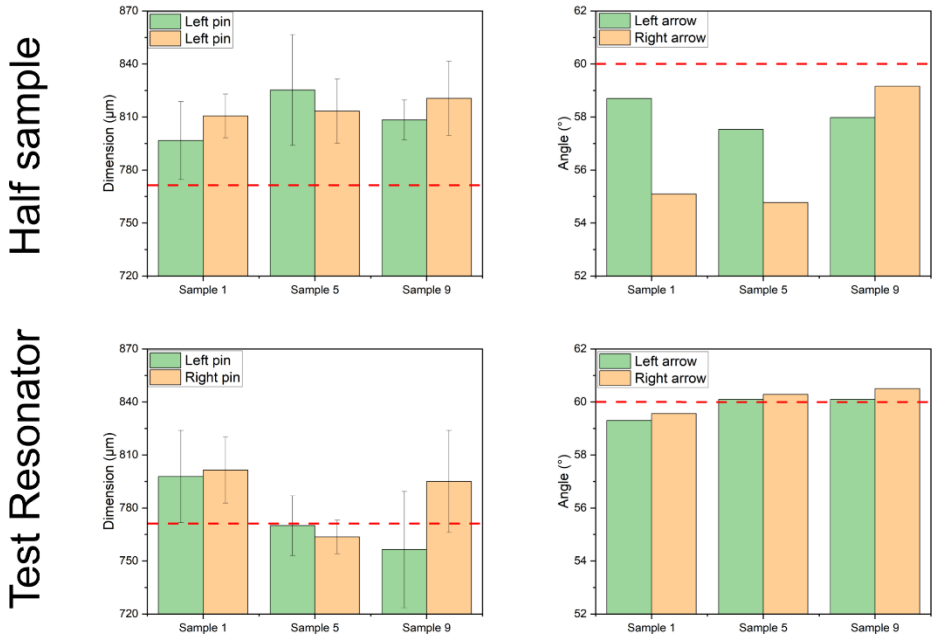

Figure 29. Dimensions in terms of thickness and angle of these arrows from half-cut component (left vertical) and test resonator (right vertical).

5.5 Effect of Melt Strategies in PBF-EB of Pure Copper (Paper VII)

To illustrate the capacity of functional components also by PBF-EB, the melt strategies to realize high performance pure copper printing by PBF-EB was explored. Figure 30 illustrates the density values of samples printed using hatch melt and point melt strategies through PBF-EB technology. A subset of samples was selected from a broader parameter range encompassing both strategies, with inclusion of specimens exhibiting the highest density value. Each sample was produced using four distinct parameters for the hatch melt and three for the point melt strategy. These combinations were assigned levels from 1 to 4. The parameters used during processing are beam current, voltage, exposure time, speed, spot distance, line offset. Area energy density (A_E), a measured value from these variables is considered in this study. Hatch melt sample 1 achieved relative densities obtained 99.6% at levels 1and 2 with A_E of 2 J/mm^2. These density values were measured through image analysis **(Figure 30(a))**. Similarly, as seen in **Figure 30(b)**, point melt samples 1 and 3 attained relative densities of 99.7% at level 2 with A_E of 11.85 J/mm^2 and 99.9% at level 3 with A_E of 9.97 J/mm^2, respectively.

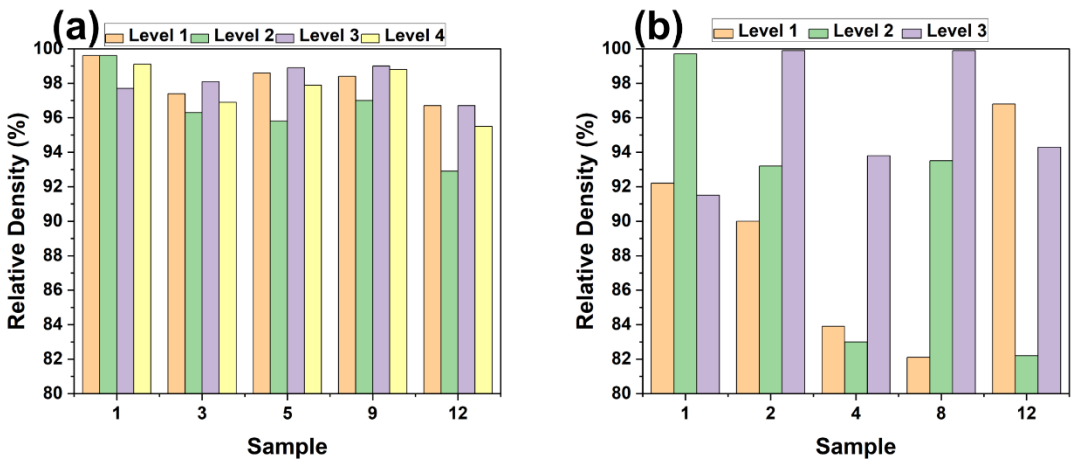

Figure 30. Relative density values of samples printed using (a) hatch melt (b) point melt strategies.

The optimized parameters resulting in higher densities were employed for the fabrication of samples intended for functional testing, including thermal and electrical conductivity measurements **(Figure 31)**. Sample 5 exhibited a thermal conductivity of 400 W/(m K) **(Figure 31(a))** and an electrical conductivity of 57.59±0.15 MS/m **(Figure 31(b))**, approximating the expected values of pure copper of 400 W/(m K) and 59 MS/m, respectively [123]. In this study, the correlation between density, microstructure on thermal and electrical conductivity was investigated. Thermal conductivity measurements conducted at intervals of 40 °C from 20 °C to 260 °C demonstrated a decreasing trend, consistent with the established literature data [124].

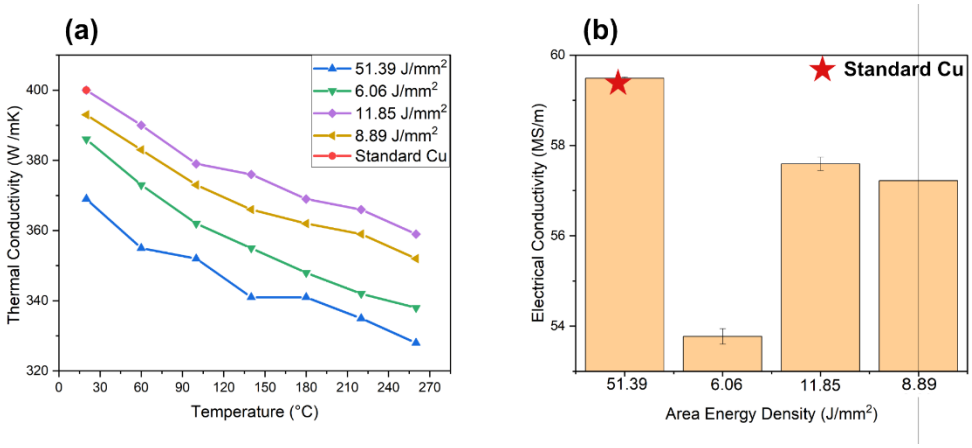

Figure 31. Measurement of (a) thermal conductivity using laser flash analysis (LFA), (b) electrical conductivity using Eddy current measurements of PBF-EB processed pure copper.

CHAPTER 6

Conclusions

The overall aim of this thesis has been to explore powder metallurgical (PM) and additive manufacturing (AM) routes to fully densify water-atomized and gas-atomized powder for structural applications and functional applications without compromising potential near-net shape capabilities. The study has addressed key research questions as outlined in the Introduction section. Below, conclusions are presented related to these research questions.

How can processing route be tailored to achieve full densification using Cr-alloyed water atomized steel powder?

- Density measurement of Cr-alloyed PM steel following capsule-free HIP revealed a relative density of 96% for sample sintered at 1150 °C and a significantly higher relative density of 99.7% for those sintered at 1250 °C. These findings emphasize the importance of high sintering temperatures as a means of setting the density of the material to enable the capsule-free HIP process.
- The CIP samples of Cr-alloyed steel exhibiting lower green density consistently displayed both open and closed porosity, after sintering at all temperatures, even following capsule-free HIP. Only CIP samples processed with minimum 600MPa were hence suitable for the intended process route involving sintering and capsule-free HIP.
- The novel processing route was shown to allow sintering and capsule-free HIP in a combined process. A density of 7.84 g/cm^3 (equivalent to 99.7% of relative density) was attained following a sintering process at 1250 °C in HIP furnace, subsequently followed by a capsule-free HIP treatment at 1150 °C.

How will alloying by admixing (Ni) affect sintering of Cr alloyed water atomized steel powder?

- The addition of 2 wt.% Ni to the Cr-alloyed PM steel significantly influenced the processing behaviour of the material towards pre-HIP densification.
- When sintering Cr-alloyed steel powder with admixed Ni, the Ni is found to activate the formation of sinter necks during the heating stage, resulting in a slight

but significant increase in overall densification, corresponding to up to 0.1% higher total shrinkage depending on sintering temperature.

- Admixed Ni, Cr-alloyed steel powder (CrA) hence showed enhanced densification, particularly when sintered at elevated temperatures (1250 °C). This resulted in a density of 7.28 g/cm^3 from an initial green density of 7.1 g/cm^3 . This level of sintered density is suitable for subsequent capsule-free HIP.
- Both CrA-0.3C and CrA-02Ni-0.3C compositions exhibited significant mass loss during heating stage of sintering, indicative of effective surface oxide reduction. This was facilitated by hydrogen from the $90N_2/10H_2$ sintering atmosphere at lower temperatures of 350-450°C to remove the Fe-oxide. Additionally, carbothermal reduction reactions, prevalent at higher temperatures (>900 °C), contribute substantially to oxygen removal and removal of more stable oxide products.
- The presence of nickel, distributed as nickel-rich regions as well as within the steel matrix, promotes the formation of bainite during cooling. This microstructural evolution significantly enhances both hardness and impact toughness. The presence of Ni is hence an important contributor to the heat treatability, including as well post-sintering carburizing.

How can processing route and sintering be tailored to achieve full density components starting from gas-atomized Vanadis 4E tool steel powder and FeCrAl powder?

Cold Work PM tool Steel

- Gas-atomized Vanadis 4E powder was transformed into granules through freeze-drying process and subsequently isostatically compacted into coherent green parts.
- Density measurements revealed values of 7.80±0.01 g/cm^3 for samples sintered at 1150 °C and subsequently subjected to capsule-free HIP, hardening, and tempering. Notably, a similar density of 7.81±0.01 g/cm^3 was achieved solely through sintering at 1200 °C prior to post-heat treatment processes.
- The densification during sintering can be assigned to the benefit of sintering in nitrogen atmosphere, which leads to the absorption of nitrogen in the material, selectively captured in MX precipitates, formed by transformation of VC-type of precipitates.
- The EDS mapping analysis of the sintered samples indicated a positive correlation between sintering temperature and the size of vanadium and molybdenum-rich precipitates.
- The former ones were expected from thermodynamic simulations and assigned to be MX-precipitates (V-rich carbonitrides), while the latter ones were assigned to be Mo-rich carbides, presumably triggered by local carbon enrichment during sintering.
- Fully densified and tempered samples exhibited higher apparent hardness when initially sintered at 1150 °C (519±14 HV10) compared to those sintered at 1200 °C

(457±11 HV10). This enhancement is attributed to a finer distribution of secondary phase precipitates in the former condition.

FeCrAl

- Freeze granulation was successfully employed to produce granules from gas-atomized FeCrAl powder that were subsequently isostatically compacted into coherent green parts.
- Sintering in pure hydrogen at high temperatures of 1400 °C and 1450 °C yielded relative densities of 99% and 99.6%, respectively. A sintering temperature of 1350 °C resulted in a relative density exceeding 96%, a threshold typically associated with the closure of surface porosity.
- Unstable oxides were reduced during sintering, while the residual oxygen level of about 0.25 wt.% was connected to the stable Al_2O_3 phase remaining in the form of finely dispersion oxide particles of micrometer size or less. The presence of these oxide particles is a wanted effect as it leads to possible grain size control and potential dispersion strengthening effect.

What are the challenges in producing precision components for functional applications using PBF-LB with particular reference to waveguides?

- Dimensional measurements of the fine-featured arrows on test resonator samples closely approximated to nominal specifications, such as width of 770 µm and angle of 60°. Conversely, half-cut samples, exhibiting greater exposure during the printing process, demonstrated increased deviations from nominal values, likely attributed to the influence of recoating and powder spreading.
- An evident correlation between geometrical deviations and resonator RF performance was not identified. Measured resonance frequencies ranged from 28.8 GHz to 29.1 GHz. Consequently, scaling of the design may effectively mitigate the impact of systematic deviations from the nominal 27.9 GHz value.
- Part-to-part variations were relatively low in comparison to the overall systematic deviation.

What is the effect of melt strategies (hatch vs. point) in powder bed fusion – electron beam (PBF-EB) on the densification, thermal and electrical conductivities?

- Pure copper samples fabricated using the hatch melt strategy allowed to a relative density of 99.5% for selected samples. Comparatively, the point melt strategy yielded a relative density of 99.7%.
- Further parameter optimization allowed to reach point melt strategy, producing components with near full density exhibiting thermal conductivity of 400 W/mK and electrical conductivity of 57.59±0.15 MS/m, respectively. These values compare with the expected levels of pure Cu.

CHAPTER 7

Future Scope

Based on the presented results and conclusions, the following recommendations are suggested to explore the studied processing routes of PM and AM technologies.

- The isotropy of material properties within CIP samples should be investigated.
- Computational modelling of CIP mould design is required to optimize shape and mould wall thickness for the enhancement of green compact densification and reaching required geometries and tolerances of the final components.
- There is need for manufacture and development of dimensional tolerance of gear shape demonstrators using CIP with 3D-printed polymer moulds for structural applications.
- There should be an economic evaluation of a novel approach combining cold isostatic pressing (CIP), with sintering in hot isostatic pressing (HIP) furnace, followed by capsule-free HIP.
- Further microstructural investigation of cold work PM tool steel material is suggested to understand the phase formations in more detail and tune the processing parameters to achieve improved tempering of martensite.
- There should be further studies of more complex geometrical features of precision components using PBF-LB for functional applications, involving the establishment of a state-of the art framework for design for PBF-LB.
- Further efforts should be addressed to investigate the impact of surface roughness of pure copper on the conductivity behaviour when processed by PBF-EB.

Acknowledgements

I would like to thank my supervisors Prof. Lars Nyborg and Prof. Eduard Hryha for believing in me and providing me with this opportunity and support to carry out research in powder metallurgy. I would like to extend my thanks to Prof. Yu Cao for providing guidance.

I am grateful to Dr. Maheswaran Vattur Sundaram (Höganäs AB) and Dr. Giulio Maistro (UddeholmsAB/Volvo Trucks) for your support and discussions of my work. I would like to acknowledge and thank all my co-authors Dr. Erik Adolfsson (RISE IVF), Mr. Johannes Gårdstam (Quintus Technologies AB), Dr. Hans Magnusson (Swerim AB), Mr. Roger Berglund (Kanthal AB) and Dr. Phillip Mahoney (Collibrium Additive) for all the collaborations within the framework of this work. I would like to acknowledge Dr. Yiming Yao, Roger Saghdahl, Dr. Eric Tam, Jonny Olausson for their availability and all the help in fixing things related technical issues whenever needed.

I would like to thank my office mate, Sajjad for your encouragement, support and for our endless conversations about investments in crypto, which we did and failed successfully. I would especially like to express my thanks to all fellow PhD students, past and present for sharing this journey with me, especially Camille, Bala, Fardan, Sahith, Vishnu, Satya, Antonio, Ezgi, Sylwia, Angelica, Plinio, Rasmus, Markus, Erika T, Dmitri and many others for their friendships, good times, and laughter.

A big thanks go to my friends, Igor and Maa, for their love, kindness, and support during my times in Germany. I would like to thank all my friends, Satish, RP, Hari, Karthik, Afshan, Paddu, Bindu, Vasu, Rasool, for sharing all those memorable moments that we had, and I won't miss a chance to have many more good times with you all.

Special thanks go to my Amma and Dad for their love, guidance, sacrifices and being on my side always have been the foundation of everything I am today. Big thanks to Akka and Bava, for your love and support, and being such incredible pillars of strength during difficult times especially while I am far away from home. Thanks to my amazing nephew, Rizi, for his love and for always inspiring me with endless questions on any topic.

To my lovely wife Preethi, I want to thank you for your unwavering support and love. I admire your patience and steadfast encouragement for me during all the difficult times. You are my solid rock of strength. This journey and accomplishment would have been impossible without you. Eager to embark on new adventures together.

Anok Babu Nagaram July 30, 2024

References

[1] "Powder Metallurgy Market Size, Share & Trends Analysis Report By Material (Titanium, Steel), By Process (MIM, PM HIP), By Application (Automotive, Oil & Gas), By End-use (OEM, AM Operators), By Region, And Segment Forecasts, 2023 - 2030," *Powder Metallurgy Market Size, Share & Growth Report*, pp. 1–7, 2023.

[2] W. Hearn, "Development of Structural Steels for Powder Bed Fusion – Laser Beam," Ph.D. Thesis, Chalmers University of Technology, Sweden, 2023. [Online]. Available: https://research.chalmers.se/publication/534092%0Ahttps://research.chalmers.se/publication/534092/file/534092_Fulltext.pdf

[3] Höganäs AB, *Höganäs Handbook for Sintered Components: Iron and Steel Powders for Sintered Components*. 2017. [Online]. Available: www.hoganas.com/pmc%0Ahttps://www.hoganas.com/globalassets/uploaded-files/handbooks/handbook-0_interactive_version_iron-and-steel-powders-for-sintered-components_2017_1840hog.pdf

[4] "Additive Manufacturing Market Size, Share & Trends Analysis Report By Component, By Printer Type, By Technology, By Software, By Application, By Vertical, By Material, By Region, And Segment Forecasts, 2024 - 2030," *Additive Manufacturing Market Size, Share & Trends Analysis Report*, pp. 1–12, 2024.

[5] J. Capus, "Higher density, higher performance at POWDERMET2018," *Metal Powder Report*, vol. 73, no. 6, pp. 310–313, 2018, doi: 10.1016/j.mprp.2018.09.002.

[6] G. F. Bocchini, "The influences of porosity on the characteristics of sintered materials," *SAE Technical Papers*, no. May, 1986, doi: 10.4271/860148.

[7] Höganäs, "Design and mechanical properties," *Höganäs handbook for sintered components*, vol. 3, p. 128, 2013.

[8] W. B. James and H. Corporation, "Powder Metallurgy Methods and Applications," vol. 7, 2015, doi: 10.31399/asm.hb.v07.a0006022.

[9] M. Vattur Sundaram, "Novel approaches for acheiving full density powder metallurgy steels," Ph.D. Thesis, Chalmers University of Technology, Sweden, 2019. [Online]. Available: https://research.chalmers.se/publication/508926/file/508926_Fulltext.pdf%0Ahttps://research.chalmers.se/publication/508926

[10] M. Ahlfors, "Heat treatment with unpreceded possibilities and flexibility," *Advances in Powder Metallurgy and Particulate Materials - 2014, Proceedings of the 2014 World Congress on Powder Metallurgy and Particulate Materials, PM 2014*, no. May 2014, pp. 3276–3281, 2014.

[11] A. P. Fagundes, J. O. D. B. Lira, N. Padoin, C. Soares, and H. G. Riella, “Additive manufacturing of functional devices for environmental applications: A review,” *J Environ Chem Eng*, vol. 10, no. 3, 2022, doi: 10.1016/j.jece.2022.108049.

[12] H. Cao and M. Wessén, “Effect of Microstructure on Mechanical Properties of As-Cast Mg-Al Alloys,” *Metall Mater Trans A Phys Metall Mater Sci*, vol. 35 A, no. 1, pp. 309–319, 2004, doi: 10.1007/s11661-004-0132-6.

[13] Höganäs AB, “Höganäs handbook for sintered components,” vol. 6, pp. 1–127, 2016.

[14] X. Zhou, H. Fang, R. Li, and T. Yuan, “Microstructure, mechanical properties and corrosion resistance of low-cost Ti–Al–Cr–Fe alloys processed via powder metallurgy,” *Mater Chem Phys*, vol. 317, no. March, p. 129197, 2024, doi: 10.1016/j.matchemphys.2024.129197.

[15] G. Matula, T. Jardiel, R. Jimenez, B. Levenfeld, and a Várez, “Microstructure , mechanical and electrical properties of Ni-YSZ anode supported solid oxide fuel cells,” *Powder Metallurgy*, vol. 32, no. 1, pp. 21–24, 2008.

[16] F. Shang, B. Qiao, H. Li, Y. He, X. Tang, and J. Yang, “Application of PM technology on manufacturing of automotive parts,” *Proceedings - 3rd International Conference on Measuring Technology and Mechatronics Automation, ICMTMA 2011*, vol. 1, pp. 563–565, 2011, doi: 10.1109/ICMTMA.2011.143.

[17] M. Haydn, K. Ortner, T. Franco, N. H. Menzler, A. Venskutonis, and L. S. Sigl, “Development of metal-supported solid oxide fuel cells based on a powder-metallurgical manufacturing route,” *International Powder Metallurgy Congress and Exhibition, Euro PM 2013*, 2013.

[18] R. Bureš, M. Strečková, M. Fáberová, P. Kollár, and J. Füzer, “Advances in Powder Metallurgy Soft Magnetic Composite Materials,” *Archives of Metallurgy and Materials*, vol. 62, no. 2, pp. 1149–1154, 2017, doi: 10.1515/amm-2017-0168.

[19] H. G. Rutz and F. G. Hanejko, “High density processing of high performance ferrous materials,” in *International Conference & Exhibition of Powder Metallurgy & Particulate Materials*, Canada, 1994.

[20] Y. Duan, W. Zhu, W. Liu, Y. Ma, Q. Cai, and Y. Cai, “A novel strategy for preparing high-performance powder metallurgical low alloy ultrahigh strength steel,” *Materials Science and Engineering: A*, vol. 864, no. January, p. 144585, 2023, doi: 10.1016/j.msea.2023.144585.

[21] C. R. Sohar, A. Betzwar-Kotas, C. Gierl, B. Weiss, and H. Danninger, “PM tool steels push the edge in fatigue tests,” *Metal Powder Report*, vol. 64, no. 2, pp. 12-13,15-17, 2009, doi: 10.1016/S0026-0657(09)70013-X.

[22] F. G. Wilson, B. R. Knott, and C. D. Desforges, “Preparation and properties of some ODS Fe-Cr-Al alloys,” *Metallurgical Transactions A*, vol. 9, no. 2, pp. 275–282, 1978, doi: 10.1007/BF02646711.

[23] R. A. Sobieszek, “Sculpture as the Sum of Its Profiles: François Willème and Photosculpture in France, 1859–1868,” *Art Bull*, vol. 62, no. 4, pp. 617–630, 1980, doi: 10.1080/00043079.1980.10787818.

[24] “ASME Historic Mechanical Engineering Landmark,” USA, 2016. [Online]. Available: https://www.asme.org/wwwasmeorg/media/resourcefiles/aboutasme/who we are/engineering history/landmarks/261-stereolithography.pdf

[25] F. M. Mwema and E. T. Akinlabi, “Basics of Fused Deposition Modelling (FDM) BT - Fused Deposition Modeling: Strategies for Quality Enhancement,” Springer, 2020, ch. Springer B, pp. 1–15. [Online]. Available: https://doi.org/10.1007/978-3-030-48259-6_1

[26] I. Yadroitsev, A. Du Plessis, and I. Yadroitsava, “Fundamentals of Laser Powder Bed Fusion of Metals,” in *Fundamentals of Laser Powder Bed Fusion of Metals*, Elsevier Inc., 2021, ch. Basics of, pp. 15–38. doi: 10.1016/B978-0-12-824090-8.00024-X.

[27] Y. J. Kim, H. N. Kim, and D. Y. Kim, “A study on effects of curing and machining conditions in post-processing of SLA additive manufactured polymer,” *J Manuf Process*, vol. 119, no. March, pp. 511–519, 2024, doi: 10.1016/j.jmapro.2024.03.112.

[28] J. Izdebska-Podsiadły, “Classification of 3D printing methods,” in *Polymers for 3D Printing: Methods, Properties, and Characteristics*, Elsevier Inc., 2022, ch. Classifica, pp. 23–34. doi: 10.1016/B978-0-12-818311-3.00009-4.

[29] J. Frketic, T. Dickens, and S. Ramakrishnan, “Automated manufacturing and processing of fiber-reinforced polymer (FRP) composites: An additive review of contemporary and modern techniques for advanced materials manufacturing,” *Addit Manuf*, vol. 14, pp. 69–86, 2017, doi: 10.1016/j.addma.2017.01.003.

[30] L. Lu, Y. Shen, X. Chen, L. Qian, and K. Lu, “Ultrahigh Strength and High Electrical Conductivity in Copper,” *Science (1979)*, vol. 304, no. 5669, pp. 422–426, 2004, doi: 10.1126/science.1092905.

[31] O. Miclette, R. Côté, V. Demers, and V. Brailovski, “Material extrusion additive manufacturing of low-viscosity metallic feedstocks: Performances of the plunger-based approach,” *Addit Manuf*, vol. 60, no. October, p. 103252, 2022, doi: 10.1016/j.addma.2022.103252.

[32] A. Elkaseer, K. J. Chen, J. C. Janhsen, O. Refle, V. Hagenmeyer, and S. G. Scholz, “Material jetting for advanced applications: A state-of-the-art review, gaps and future directions,” *Addit Manuf*, vol. 60, no. PA, p. 103270, 2022, doi: 10.1016/j.addma.2022.103270.

[33] D. Svetlizky *et al.*, “Directed energy deposition (DED) additive manufacturing: Physical characteristics, defects, challenges and applications,” *Materials Today*, vol. 49, no. December 2022, pp. 271–295, 2021, doi: 10.1016/j.mattod.2021.03.020.

[34] S. Hoeges, A. Zwiren, and C. Schade, “Additive manufacturing using water atomized steel powders,” *Metal Powder Report*, vol. 72, no. 2, pp. 111–117, 2017, doi: 10.1016/j.mprp.2017.01.004.

[35] M. R. Jandaghi, H. Pouraliakbar, L. Iannucci, V. Fallah, and M. Pavese, “Comparative assessment of gas and water atomized powders for additive manufacturing of 316 L stainless steel: Microstructure, mechanical properties, and corrosion resistance,” *Mater Charact*, vol. 204, no. July, p. 113204, 2023, doi: 10.1016/j.matchar.2023.113204.

[36] E. Hryha and L. Nyborg, “Oxide transformation in Cr-Mn-prealloyed sintered steels: Thermodynamic and kinetic aspects,” *Metall Mater Trans A Phys Metall Mater Sci*, vol. 45, pp. 1736–1747, 2014, doi: 10.1007/s11661-013-1969-3.

[37] D. Chasoglou, E. Hryha, M. Norell, and L. Nyborg, “Characterization of surface oxides on water-atomized steel powder by XPS/AES depth profiling and nano-scale lateral surface analysis,” *Appl Surf Sci*, vol. 268, pp. 496–506, 2013, doi: 10.1016/j.apsusc.2012.12.155.

[38] E. Hryha, C. Gierl, L. Nyborg, H. Danninger, and E. Dudrova, “Surface composition of the steel powders pre-alloyed with manganese,” *Appl Surf Sci*, vol. 256, no. 12, pp. 3946–3961, 2010, doi: 10.1016/j.apsusc.2010.01.055.

[39] P. Moghimian *et al.*, “Metal powders in additive manufacturing: A review on reusability and recyclability of common titanium, nickel and aluminum alloys,” *Addit Manuf*, vol. 43, no. March, p. 102017, 2021, doi: 10.1016/j.addma.2021.102017.

[40] C. Schade and J. J. Dunkley, “Atomization,” *Powder Metallurgy*, vol. 7, pp. 58–71, 2018, doi: 10.31399/asm.hb.v07.a0006084.

[41] Christer Åslund, “Dense parts produced by uniaxial compressing an agglomerated spherical metal powder,” 2002 [Online]. Available: https://patentimages.storage.googleapis.com/30/f4/62/e9b75605352fb0/US10679987.pdf

[42] W. B. James, “Ferrous Powder Metallurgy Materials,” *Powder Metallurgy*, vol. 7, pp. 295–310, 2018, doi: 10.31399/asm.hb.v07.a0006101.

[43] M. Nabee, R. Frykholm, and P. Hedström, “Influence of alloying elements on Ni distribution in PM steels,” *Powder Metallurgy*, vol. 57, no. 2, pp. 111–118, 2014, doi: 10.1179/1743290113Y.0000000078.

[44] S. Geroldinger, “Sinter Hardening PM Steels Prepared through Hybrid Alloying,” *HTM - Journal of Heat Treatment and Materials*, vol. 76, no. 2, pp. 105–119, 2021, doi: 10.1515/htm-2020-0007.

[45] K. Rundgren, O. Lyckfeldt, and M. Sjöstedt, “Improving Powders with Freeze Granulation,” *Ceramic Industry*, no. April, pp. 40–44, 2003.

[46] R. Haynes, “Development of sintered low alloy steels,” *Powder Metallurgy*, vol. 32, no. 2, pp. 140–146, 1989, doi: 10.1179/pom.1989.32.2.140.

[47] M. Danninger, H., Zengin, Z-O., Drozda, “High Pressure Compaction of Ferrous PM Parts,” *Metal Powder Report*, vol. 41, no. 11, pp. 833–838, 1986.

[48] N. D. Sopchak and W. Z. Misiolek, “Density gradients in multilayer compacted iron powder parts,” *Materials and Manufacturing Processes*, vol. 15, no. 1, pp. 65–79, 2000, doi: 10.1080/10426910008912973.

[49] R. M. German, “Green body homogeneity effects on sintered tolerances,” *Powder Metallurgy*, vol. 47, no. 2, pp. 157–160, 2004, doi: 10.1179/003258904225015563.

[50] Höganäs AB, “Höganäs Handbook for Sintered Components Power of Powder ® Production of Sintered Components 2,” 2013, [Online]. Available: www.hoganas.com/pmc

[51] JAMES PJ, “Cold isostatic pressing,” *Prod Eng (London)*, vol. 50, no. 12, pp. 515–520, 1971, doi: 10.31399/asm.hb.v07.a0006074.

[52] “CIP powder characteristics,” *Powder Metallurgy Review*, pp. 61–67, 2019.

[53] U. M. Attia, “Cold-isostatic pressing of metal powders: a review of the technology and recent developments,” *Critical Reviews in Solid State and Materials Sciences*, vol. 46, no. 6, pp. 587–610, 2021, doi: 10.1080/10408436.2021.1886043.

[54] R. M. Govindarajan and N. Aravas, “DEFORMATION PROCESSING OF METAL POWDERS: PART I-COLD ISOSTATIC PRESSING,” *Int. J. Mech. S6*, vol. 36, no. 4, pp. 343–357, 1994.

[55] A. Simchi, “Effects of lubrication procedure on the consolidation, sintering and microstructural features of powder compacts,” *Mater Des*, vol. 24, no. 8, pp. 585–594, 2003, doi: 10.1016/S0261-3069(03)00155-9.

[56] E. Hryha, S. Karamchedu, D. Riabov, L. Nyborg, and S. Berg, “Effect of Active Components of Sintering Atmosphere on Reduction/Oxidation Processes during Sintering of Cr-Alloyed PM Steels,” *Journal of the American Ceramic Society*, vol. 98, no. 11, pp. 3561–3568, 2015, doi: 10.1111/jace.13607.

[57] E. Hryha, H. Borgström, K. Sterky, and L. Nyborg, “Influence of the steel powder type and processing parameters on the debinding of PM compacts with gelatin binder,” *J Therm Anal Calorim*, vol. 118, no. 2, pp. 695–704, 2014, doi: 10.1007/s10973-014-3839-7.

[58] E. Hryha, E. Dudrova, and L. Nyborg, “On-line control of processing atmospheres for proper sintering of oxidation-sensitive PM steels,” *J Mater Process Technol*, vol. 212, no. 4, pp. 977–987, 2012, doi: 10.1016/j.jmatprotec.2011.12.008.

[59] E. Hryha and L. Nyborg, “Process control system for delubrication of PM steels,” *Acta Metallurgica Slovaca*, vol. 18, no. 2–3, pp. 60–68, 2012.

[60] J. Gonzalez-Gutierrez, S. Cano, S. Schuschnigg, C. Kukla, J. Sapkota, and C. Holzer, “Additive manufacturing of metallic and ceramic components by the material extrusion of highly-filled polymers: A review and future perspectives,” *Materials*, vol. 11, no. 5, pp. 1–36, 2018, doi: 10.3390/ma11050840.

[61] K. T. Kim and J. H. Cho, “A densification model for mixed metal powder under cold compaction,” *Int J Mech Sci*, vol. 43, no. 12, pp. 2929–2946, 2001, doi: 10.1016/S0020-7403(01)00062-5.

[62] N. Lecis *et al.*, “Effects of process parameters, debinding and sintering on the microstructure of 316L stainless steel produced by binder jetting,” *Materials Science and Engineering: A*, vol. 828, no. July, p. 142108, 2021, doi: 10.1016/j.msea.2021.142108.

[63] Y. Thompson, J. Gonzalez-Gutierrez, C. Kukla, and P. Felfer, “Fused filament fabrication, debinding and sintering as a low cost additive manufacturing method of 316L stainless steel,” *Addit Manuf*, vol. 30, no. May, p. 100861, 2019, doi: 10.1016/j.addma.2019.100861.

[64] R. M. German, “Coarsening in sintering: Grain shape distribution, grain size distribution, and grain growth kinetics in solid-pore systems,” *Critical Reviews in Solid State and Materials Sciences*, vol. 35, no. 4, pp. 263–305, 2010, doi: 10.1080/10408436.2010.525197.

[65] O. Bergman, D. Chasoglou, and M. Dahlström, “Properties of Cr-alloyed PM steel after different sintering and heat treatment operations,” *APMA-2017, The 4th International Conference on Powder Metallurgy in Asia, Taiwan*.

[66] Linde AG, “Sintering of steels .,” *Furnace atmospheres*, no. 6, 2020, [Online]. Available: https://www.linde-gas.com/en/images/Furnace atmospheres no. 6. Sintering of steels._tcm17-460206.pdf

[67] Z. A. Munir, “Surface oxides and sintering of metals,” *Powder Metallurgy*, vol. 24, no. 4, pp. 177–180, 1981, doi: 10.1179/pom.1981.24.4.177.

[68] E. Hryha, “Application of fractography for investigation of surface oxide reduction/transformation and inter-particle necks formation during sintering of prealloyed with Cr and Mn PM steels,” *Powder Metallurgy Progress*, vol. 14, no. 1, pp. 24–31, 2014.

[69] D. Chasoglou, E. Hryha, and L. Nyborg, “Effect of process parameters on surface oxides on chromium-alloyed steel powder during sintering,” *Mater Chem Phys*, vol. 138, no. 1, pp. 405–415, 2013, doi: 10.1016/j.matchemphys.2012.11.074.

[70] J. Wendel, R. Shvab, Y. Cao, E. Hryha, and L. Nyborg, “Surface analysis of fine water-atomized iron powder and sintered material,” *Surface and Interface Analysis*, vol. 50, no. 11, pp. 1065–1071, 2018, doi: 10.1002/sia.6455.

[71] E. Hryha and L. Nyborg, “Thermogravimetry study of the effectiveness of different reducing agents during sintering of Cr-prealloyed PM steels,” *J Therm Anal Calorim*, vol. 118, no. 2, pp. 825–834, 2014, doi: 10.1007/s10973-014-3915-z.

[72] R. M. German, P. Suri, and S. J. Park, “Review: Liquid phase sintering,” *J Mater Sci*, vol. 44, no. 1, pp. 1–39, 2009, doi: 10.1007/s10853-008-3008-0.

[73] R. M. German, *Sintering: Theory and Practice*. New York, NY, USA: A Willey-Interscience Publication, 1996.

[74] R. M. German, *Liquid Phase Sintering*. Pleneum Publishing Corporation, 1985.

[75] R. de Oro Calderon, C. Gierl-Mayer, and H. Danninger, “Fundamentals of Sintering: Liquid Phase Sintering,” *Encyclopedia of Materials: Metals and Alloys*, no. June, pp. 481–492, 2021, doi: 10.1016/B978-0-12-819726-4.00127-7.

[76] H. Danninger, R. De Oro Calderon, and C. Gierl-Mayer, “The use of transient liquid phases in powder metallurgy,” *Materials Science Forum*, vol. 1016 MSF, pp. 69–76, 2021, doi: 10.4028/www.scientific.net/MSF.1016.69.

[77] A. B. Nagaram *et al.*, “Consolidation of water-atomized chromium–nickel-alloyed powder metallurgy steel through novel processing routes,” *Powder Metallurgy*, vol. 67, no. 1, pp. 6–17, 2024, doi: 10.1177/00325899231213007.

[78] O. Bergman, D. Chasoglou, and M. Dahlström, “Mechanical performance of Cr-alloyed PM steel after different sintering and heat treatment operations,” *Metal Powder Report*, vol. 73, no. 1, pp. 21–25, 2018, doi: 10.1016/j.mprp.2017.01.003.

[79] S. Kremel, H. Danninger, and Y. Yu, “Effect of Sintering conditions on Particle contacts and mechanical properties of PM steels prepared from 3 % Cr prealloyed powder,” *Powder Metallurgy Progress*, vol. 2, no. 4, pp. 211–221, 2002.

[80] M. Campos, L. Blanco, and J. M. Torralba, “Thermal analysis of prealloyed Fe-3Cr-0.5Mo sintered steel,” *J Therm Anal Calorim*, vol. 84, no. 2, pp. 483–487, 2006, doi: 10.1007/s10973-005-6991-2.

[81] *Höganäs Handbook Sintering Chapter 6 Höganäs, Sweden*.

[82] D. F. Heaney, “Vacuum sintering,” in *Sintering of Advanced Materials*, Elsevier, 2010, pp. 189–221. doi: 10.1533/9781845699949.2.189.

[83] N.L. Loh and K.Y. Sia, “An overview of hot isostatic pressing,” *Journal of Materials Processing Tech.*, vol. 30, pp. 45–65, 1992, doi: 10.1016/0924-0136(92)90038-T.

[84] A. Flodin, M. Andersson, and A. Miedzinski, “Full density powder metal components through Hot Isostatic Pressing,” *Metal Powder Report*, vol. 72, no. 2, pp. 107–110, 2017, doi: 10.1016/j.mprp.2016.02.057.

[85] M. Vattur Sundaram, E. Hryha, D. Chasoglou, A. Rottstegge, and L. Nyborg, “Effect of Density and Processing Conditions on Oxide Transformations and Mechanical Properties in Cr–Mo-Alloyed PM steels,” *Metall Mater Trans A Phys Metall Mater Sci*, vol. 53, no. A, pp. 640–652, 2022, doi: 10.1007/s11661-021-06539-4.

[86] J. James, “Hot isostatic pressing : an economic route to powder components,” *Metals and Materials*, no. November, pp. 27–31, 1977.

[87] C. Barre, “Hot isostatic pressing,” *Advanced Materials and Processes*, vol. 155, no. 3, pp. 47–48, 1999, doi: 10.1080/09603409.1991.11689642.

[88] W. R. Morgan and R. L. Sands, “Isostatic compaction of metal powders,” *Kovove Materialy*, vol. 14, no. 1, pp. 85–102, 1969, doi: 10.1179/mtlr.1969.14.1.85.

[89] J. C. H. and C. G. H. S.J. Mashl, “Producing large P/M near-net shapes using hot isostatic pressing,” *Journal of Materials Processing Tech.*, vol. 51, no. 7, pp. 29–31, 1999, doi: 10.1007/s11837-999-0106-7.

[90] M. Andersson *et al.*, “Manufacturing full density powder metallurgy gears through HIP:ing,” *Metal Powder Report*, vol. 74, no. 4, pp. 199–203, 2019, doi: 10.1016/j.mprp.2018.12.076.

[91] A. Leicht *et al.*, “As-HIP microstructure of EBM fabricated shell components,” *World PM 2016 Congress and Exhibition*, 2016.

[92] O. Diegel, A. Nordin, and D. Motte, *Additive Manufacturing Technologies*. Springer, 2019. doi: 10.1007/978-981-13-8281-9_2.

[93] L. Haferkamp *et al.*, “The Influence of Particle Shape , Powder Flowability , Bed Fusion,” *Metals (Basel)*, vol. 11, no. 418, pp. 1–14, 2021.

[94] O. Aydin and R. Unal, “Experimental and numerical modeling of the gas atomization nozzle for gas flow behavior,” *Comput Fluids*, vol. 42, no. 1, pp. 37–43, 2011, doi: 10.1016/j.compfluid.2010.10.013.

[95] S. Lampman, “Compressibility and Compactibility of Metal Powders,” *Powder Metallurgy*, vol. 7, pp. 171–178, 2018, doi: 10.31399/asm.hb.v07.a0006032.

[96] J. Hlosta, D. Žurovec, L. Jezerská, J. Zegzulka, and J. Nečas, “Effect of particle shape and size on the compressibility and bulk properties of powders in powder metallurgy,” *METAL 2016 - 25th Anniversary International Conference on Metallurgy and Materials, Conference Proceedings*, no. May, pp. 1394–1399, 2016.

[97] S. Wang, X. Guo, H. Lu, and H. Liu, “Experimental study on the effects of particle characteristics and pressurization methods on powder compression,” *Chem Eng Sci*, vol. 260, p. 117927, 2022, doi: 10.1016/j.ces.2022.117927.

[98] B. Palanki, “Some factors affecting densification and grain growth in the sintering of uranium dioxide – a brief review,” *Journal of Nuclear Materials*, vol. 550, p. 152918, 2021, doi: 10.1016/j.jnucmat.2021.152918.

[99] E. Hjortsberg, L. Nyborg, and H. Vidarsson, “Microscopic characterisation of topography and lubricant distribution on surface of powder compacts,” *Powder Metallurgy*, vol. 48, no. 4, pp. 345–353, 2005, doi: 10.1179/174329005X73711.

[100] W. Schatt and K.-P. Wieters, *Powder Metallurgy: Processing and Materials*, European P. VDI-Verlag GmbH, 1997.

[101] M. W. Wu and K. S. Hwang, “Improved homogenization of Ni in sintered steels through the use of Cr-containing prealloyed powders,” *Metall Mater Trans A Phys Metall Mater Sci*, vol. 37, no. 12, pp. 3577–3585, 2006, doi: 10.1007/s11661-006-1052-4.

[102] S. J. Polasik, J. J. Williams, and N. Chawla, “Fatigue crack initiation and propagation of binder-treated powder metallurgy steels,” *Metall Mater Trans A Phys Metall Mater Sci*, vol. 33, no. 1, pp. 73–81, 2002, doi: 10.1007/s11661-002-0006-8.

[103] N. Chawla, J. J. Williams, X. Deng, C. Mcclimon, L. Hunter, and S. H. Lau, “Three-dimensional characterization ahd modeling of porosity in PM steels,” *International Journal of Powder Metallurgy (Princeton, New Jersey)*, vol. 45, no. 2, pp. 19–27, 2009.

[104] E. Bernardo, M. Campos, J. M. Torralba, C. Gierl, H. Danninger, and R. Frykholm, “Lean steels modified with a new Cu-based master alloy: Influence of process parameters in dimensional and sintering behavior,” *International Powder Metallurgy Congress and Exhibition, Euro PM 2013*, 2013.

[105] M. W. Wu, K. S. Hwang, and K. H. Chuang, “Improved distribution of nickel and carbon in sintered steels through addition of chromium and molybdenum,” *Powder Metallurgy*, vol. 51, no. 2, pp. 160–165, 2008, doi: 10.1179/174329007X189667.

[106] M. W. Wu, L. C. Tsao, G. J. Shu, and B. H. Lin, “The effects of alloying elements and microstructure on the impact toughness of powder metal steels,” *Materials Science and Engineering A*, vol. 538, pp. 135–144, 2012, doi: 10.1016/j.msea.2011.12.113.

[107] F. Hanejko, “Single press/single sinter solutions to high density,” *Powder Metallurgy*, vol. 53, no. 2, pp. 100–102, 2010, doi: 10.1179/174329010X12737422260377.

[108] T. Marcu, A. Molinari, G. Straffelini, and S. Berg, “Microstructure and tensile properties of 3%Cr-0·5%Mo high carbon PM sintered steels,” *Powder Metallurgy*, vol. 48, no. 2, pp. 139–143, 2005, doi: 10.1179/003258905X37701.

[109] C. Lindberg, “Mechanical properties of warm compacted astaloy CrM,” *Advances in Powder Metallurgy and Particulate Materials*, vol. 3, no. 6/9, pp. 6–81, 2000.

[110] E. Hryha and L. Nyborg, “Microstructure development in powder metallurgy steels: Effect of alloying elements and process variables,” *Materials Science Forum*, vol. 782, pp. 467–472, 2014, doi: 10.4028/www.scientific.net/MSF.782.467.

[111] Uddeholms AB, “Heat Treatment of Tool Steel,” vol. 8, pp. 1–20, 2012.

[112] R. Guschlbauer, A. K. Burkhardt, Z. Fu, and C. Körner, “Effect of the oxygen content of pure copper powder on selective electron beam melting,” *Materials Science and Engineering: A*, vol. 779, no. February, p. 139106, 2020, doi: 10.1016/j.msea.2020.139106.

[113] S. Megahed *et al.*, “Manufacturing of Pure Copper with Electron Beam Melting and the Effect of Thermal and Abrasive Post-Processing on Microstructure and Electric Conductivity,” *Materials*, vol. 16, no. 73, 2023, doi: 10.3390/ma16010073.

[114] P. V. Andrews, M. B. West, and C. R. Robeson, “The effect of grain boundaries on the electrical resistivity of polycrystalline copper and aluminium,” *Philosophical Magazine*, vol. 19, no. 161, pp. 887–898, 1969, doi: 10.1080/14786436908225855.

[115] J. Skiba, M. Kulczyk, S. Przybysz-Gloc, M. Skorupska, M. Kobus, and K. Nowak, “Effect of microstructure refinement of pure copper on improving the performance of electrodes in electro discharge machining (EDM),” *Sci Rep*, vol. 13, no. 1, pp. 1–12, 2023, doi: 10.1038/s41598-023-43584-y.

[116] L. Dong *et al.*, “Contribution of grain boundary to strength and electrical conductivity of annealed copper wires,” *Journal of Materials Research and Technology*, vol. 26, pp. 1459–1468, 2023, doi: 10.1016/j.jmrt.2023.08.012.

[117] A. Bodyakova, M. Tkachev, A. Pilipenko, A. Belyakov, and R. Kaibyshev, “Effect of deformation methods on microstructure, texture, and properties of a Cu–Mg alloy,” *Materials Science and Engineering: A*, vol. 876, no. February, p. 145126, 2023, doi: 10.1016/j.msea.2023.145126.

[118] S. Uchida *et al.*, “Microstructures and electrical and mechanical properties of Cu-Cr alloys fabricated by selective laser melting,” *Mater Des*, vol. 175, p. 107815, 2019, doi: 10.1016/j.matdes.2019.107815.

[119] N. D. Vallejo, C. Lucas, N. Ayers, K. Graydon, H. Hyer, and Y. Sohn, “Process optimization and microstructure analysis to understand laser powder bed fusion of 316l stainless steel,” *Metals (Basel)*, vol. 11, no. 832, 2021, doi: 10.3390/met11050832.

[120] X. Wang, J. A. Muñiz-Lerma, O. Sánchez-Mata, M. Attarian Shandiz, and M. Brochu, “Microstructure and mechanical properties of stainless steel 316L vertical struts manufactured by laser powder bed fusion process,” *Materials Science and Engineering: A*, vol. 736, no. August, pp. 27–40, 2018, doi: 10.1016/j.msea.2018.08.069.

[121] A. Leicht, “Laser powder bed fusion of 316L stainless steel : microstructure and mechanical properties as a function of process parameters, design and productivity,” Ph.D. Thesis, Chalmers University of Technology, Sweden, 2020.

[122] A. B. Nagaram *et al.*, “Effect Of Process Control On The Densification Of Cr-Prealloyed PM Steels Through Vacuum Sintering In Conjunction With Capsule-Free Hot Isostatic Pressing,” in *World PM 2022 Congress Proceedings*, 2022.

[123] S. J. Raab, R. Guschlbauer, M. A. Lodes, and C. Körner, “Thermal and Electrical Conductivity of 99.9% Pure Copper Processed via Selective Electron Beam Melting,” *Adv Eng Mater*, vol. 18, no. 9, pp. 1661–1666, 2016, doi: 10.1002/adem.201600078.

[124] R. L. Powell, W. M. Rogers, and H. M. Roder, “Thermal Conductivities of copper and copper alloys,” *Adv Cryog Eng*, vol. 2, pp. 166–171, 1960, doi: https://doi.org/10.1007/978-1-4684-3102-5_28.